arXiv:0901.3372v1 [astro-ph.CO] 21 Jan 2009

Preprint typeset using LaTeX style emulateapj v. 10/09/06

COSMIC EVOLUTION OF RADIO SELECTED ACTIVE GALACTIC NUCLEI IN THE COSMOS FIELD[0]

V. Smolčić[1], G. Zamorani[2], E. Schinnerer[3], S. Bardelli[2], M. Bondi[4], L. Bîrzan[5,6], C. L. Carilli[7], P. Ciliegi[2], O. Ilbert[8], A. M. Koekemoer[9], A. Merloni[10,11] T. Paglione[12,13], M. Salvato[1], M. Scodeggio[14], N. Scoville[1]

ABSTRACT

We explore the cosmic evolution of radio AGN with low radio powers ($L_{1.4\mathrm{GHz}} \lesssim 5 \times 10^{25}$ W Hz^{-1}) out to $z = 1.3$ using to-date the largest sample of ~ 600 low luminosity radio AGN at intermediate redshift drawn from the VLA-COSMOS survey. We derive the radio luminosity function for these AGN, and its evolution with cosmic time assuming two extreme cases: i) pure luminosity and ii) pure density evolution. The former and latter yield $L_* \propto (1+z)^{0.8\pm0.1}$, and $\Phi_* \propto (1+z)^{1.1\pm0.1}$, respectively, both implying a fairly modest change in properties of low radio-power AGN since $z = 1.3$. We show that this is in stark contrast with the evolution of powerful ($L_{1.4\mathrm{GHz}} > 5 \times 10^{25}$ W Hz^{-1}) radio AGN over the same cosmic time interval, constrained using the 3CRR, 6CE, and 7CRS radio surveys by Willott et al. (2001). We demonstrate that this can be explained through differences in black hole fueling and triggering mechanisms, and a dichotomy in host galaxy properties of weak and powerful AGN. Our findings suggest that high and low radio-power AGN activity is triggered in different stages during the formation of massive red galaxies. We show that weak radio AGN occur in the most massive galaxies already at $z \sim 1$, and they may significantly contribute to the heating of their surrounding medium and thus inhibit gas accretion onto their host galaxies, as recently suggested for the 'radio mode' in cosmological models.

Subject headings: galaxies: fundamental parameters – galaxies: active, evolution – cosmology: observations – radio continuum: galaxies

1. INTRODUCTION

1.1. *AGN feedback: The impact of radio sources on galaxy formation*

Radio activity from active galactic nuclei (AGN) has recently been invoked in cosmological models as a significant ingredient in the process of galaxy formation ('AGN feedback'). Given that, in the past, cosmological models led to a systematic over-prediction of the high-mass end of the galaxy stellar mass function (e.g. White & Rees 1978; White & Frenk 1991), the implementation of gas heating through energetic radio outflows – the 'radio' mode[16] – managed to reproduce well many observed galaxy properties (e.g. the galaxies' stellar mass function, color bimodality; Croton et al. 2006, Bower et al. 2006). The particular choice of a 'radio mode' as the relevant heating mechanism has been motivated by many observational results verifying the interplay between the emission of radio galaxies in galaxy clusters, and the cluster's hot X-ray emitting gas on large-scales (e.g. Fabian et al. 2003, Forman et al. 2005).

In the centers of galaxy clusters the radiative cooling time of the intra-cluster medium (ICM) is shorter than the age of the cluster. Thus, the central ICM is expected to be significantly colder compared to outskirt-regions (such clusters are referred to as 'cooling flow clusters'). However, generally the expected cool X-ray phases are not observed, and this is known as the 'cooling flow problem'. The most likely solution to this problem is thought to be radio galaxies as it is usually observed that the synchrotron plasma ejected by their radio jets inflates bubbles in the hot X-ray emitting cluster gas and thereby heats it (see Fabian 1994 for a review). In theoretical models, a similar interplay on smaller scales has been assumed to be at work between the radio outflows of a galaxy and its surrounding hot gas halo.

The first observational evidence for the 'radio mode' feedback in the context of galaxy formation has been found by Best et al. (2006). Based on X-ray and radio observations of a local sample of massive elliptical galaxies (Best et al. 2005) they have shown that the radio source heating may indeed balance the radiative energy losses from the hot gas surrounding the galaxy, as postulated in the models. Based on an independent

---

[0] Based on observations with the National Radio Astronomy Observatory which is a facility of the National Science Foundation operated under cooperative agreement by Associated Universities, Inc.

[1] California Institute of Technology, MC 105-24, 1200 East California Boulevard, Pasadena, CA 91125

[2] INAF - Osservatorio Astronomico di Bologna, via Ranzani 1, 40127, Bologna, Italy

[3] Max Planck Institut für Astronomie, Königstuhl 17, Heidelberg, D-69117, Germany

[4] INAF - Istituto di Radioastronomia, via Gobetti 101, 40129 Bologna, Italy

[5] Department of Astronomy and Astrophysics, Pennsylvania State University, University Park, PA 16802

[6] Department of Physics and Astronomy, Ohio University, Clippinger Laboratories, Athens, OH 45701

[7] National Radio Astronomy Observatory, P.O. Box 0, Socorro, NM 87801-0387

[8] Institute for Astronomy, 2680 Woodlawn Dr., University of Hawaii, Honolulu, Hawaii, 96822

[9] Space Telescope Science Institute, 3700 San Martin Drive, Baltimore, MD 21218

[10] Excellence Cluster Universe, Technische Universitt Mnchen, Boltzmannstr. 2, D-85748, Garching, Germany

[11] Max-Planck-Institut für Extraterrestrische Physik, Giessenbachstr., D-85741 Garching, Germany

[12] York College, City University of New York, 94-20 Guy R. Brewer Boulevard, Jamaica, NY 11451

[13] American Museum of Natural History, Central Park West at 79th Street, New York, NY 10024

[14] IASF Milano-INAF, Via Bassini 15, I-20133, Milan, Italy

[16] The 'radio mode' is defined here as given in Croton et al. (2006).

sample of radio galaxies in galaxy clusters (studied by Bîrzan et al. 2004) Best et al. (2006) have correlated the mechanical heating provided by the radio sources on their surrounding medium with monochromatic 20 cm radio power. Combining this with the local radio AGN luminosity function (Best et al. 2005), they have found that the volume-averaged mechanical energy heating rate of local radio luminous AGN is about a factor of 10-20 lower than predicted by the Croton et al. (2006) model. They assigned this difference to a systematic over-prediction of the heating rate in the model (by a factor of 2-3) and the intention of the model to jointly describe both the large- and small- scale heating from radio sources (i.e. on both cluster and galaxy scales). More recent calculations of the volume averaged mechanical energy heating rate due to AGN (Körding et al. 2008; Merloni & Heinz 2008) yield higher values at $z = 0$ compared to the results of Best et al. (2006), and thus closer to the Croton et al. (2006) prediction.

To date no clear picture exists on how the AGN radio mode feedback works. More observations are needed to provide better constraints on the physics of this process, as well as its evolution with cosmic time. Here we attempt to shed light on the latter utilizing a large statistical sample of radio AGN, drawn from the VLA-COSMOS survey (Schinnerer et al. 2007).

1.2. *Radio luminous AGN and their evolution*

Fanaroff & Riley (1974, FR hereafter) were the first to note that the radio luminous AGN population consists of two apparently distinct types of sources, referred to as FR type I and II, with prominent differences in both radio morphology and luminosity. The radio emission from FR I radio galaxies is core dominated, while FR IIs are edge-brightened with highly collimated large-scale jets. FR IIs are typically more powerful in the radio than FR Is, and a dividing luminosity of $L_{178\mathrm{MHz}} \sim 2.5 \times 10^{26}$ W Hz^{-1} (corresponding to $L_{1.4\mathrm{GHz}} \sim 6 \times 10^{25}$ W Hz^{-1})[17] has been suggested (Fanaroff & Riley 1974). It has been later shown (Ledlow & Owen 1996) that the FR I/FR II division is also a function of the host galaxy optical luminosity (with a higher dividing radio luminosity for higher optical host luminosity).

An alternative way of classifying radio AGN is based on the existence of high excitation (HE) emission lines in the optical spectra of their host galaxies (Hine & Longair 1979; Laing et al. 1994). In this scheme, objects without high-excitation emission lines are referred to as low-excitation (LE) radio galaxies, and they are most common at low radio luminosities. Almost all FR I radio galaxies are LE sources, while optical hosts of the most powerful radio sources, i.e. FR IIs, usually have strong emission lines. It is noteworthy, however, that the correspondence between the FR class and the presence of emission lines is not one-to-one. Many FR II galaxies have been found to be low-excitation radio galaxies (e.g. Evans et al. 2006).

Recently, strong evidence (Evans et al. 2006; Hardcastle et al. 2006, 2007) has emerged supporting the idea that low- and high- excitation radio AGN (hereafter LERAGN and HERAGN, respectively) reflect different modes of black hole (BH) accretion. Independent studies have shown that i) LERAGN are a class of radio luminous AGN that accrete radiatively inefficiently (Evans et al. 2006; Hardcastle et al. 2006), and ii) Bondi accretion of the hot X-ray emitting intergalactic medium (IGM) is sufficient to power the jets of low-power radio galaxies in the centers of galaxy clusters (based on a sample of nearby galaxies; Allen et al. 2006). Based on these findings Hardcastle et al. (2007) have developed a model in which all low-excitation radio sources are powered by radiatively inefficient accretion (i.e. at sub-Eddington accretion rates) of the hot phase of the IGM, while high-excitation sources are powered by radiatively efficient accretion (at $\sim$ Eddington rates) of cold gas (that is in general unrelated to the hot IGM; see also Merloni & Heinz 2008). This model successfully explains a variety of properties of radio luminous AGN, such as their environments, signs of galaxy mergers in the hosts of powerful (high-excitation) radio sources, and the break of the radio AGN luminosity function (for details see Hardcastle et al. 2007 and references therein).

In the past two decades it has become clear that radio luminous AGN evolve differentially: Low-power sources evolve less strongly than high-power sources. Numerous studies of high luminosity radio AGN ($L_{2.7\mathrm{GHz}} \gtrsim 10^{25}$ W Hz^{-1} sr^{-1} corresponding to $\mathrm{L}_{1.4\mathrm{GHz}} \sim 2 \times 10^{26}$ W Hz^{-1}; Dunlop & Peacock 1990; Willott et al. 2001) have found a strong positive density evolution with redshift of these sources out to a redshift peak of $z \sim 2$. Beyond this redshift their comoving volume density starts declining (a possible sharp density cut-off has been suggested by Dunlop & Peacock 1990, but has not been confirmed by Willott et al. 2001). Such a decline would be consistent with the results obtained via optical surveys (Schmidt et al. 1995) and, recently, X-ray surveys (Silverman et al. 2008; Brusa et al. 2008).

Analyzing the evolution of lower-power radio AGN ($\mathrm{L}_{1.4\mathrm{GHz}} > 2 \times 10^{25}$ W Hz^{-1}) Waddington et al. (2001) have found a significantly slower evolution of this population, with the comoving volume density turn-over occurring at a lower redshift ($z \sim 1 - 1.5$), compared to the high-power radio population. Different radio-optical surveys are still somewhat controversial. While Clewley & Jarvis (2004) and Sadler et al. (2007) find no evidence for particularly *strong* evolution out to $z \sim 0.7$, Cowie et al. (2004) have found a strong density evolution out to $z \sim 1.5$. Thus, although on average a weaker evolution of low-power (compared to high-power) radio AGN is implied, it is still not very well understood how the low-luminosity radio AGN evolve with redshift. In this work we use the VLA-COSMOS AGN sample of low luminosity (96% have $\mathrm{L}_{1.4\mathrm{GHz}} < 10^{25}$ W Hz^{-1}) radio sources in order to comprehensively constrain the evolution of the low-power radio AGN out to $z = 1.3$. We combine our results with the new findings and ideas on the cosmological relevance of radio AGN in order to study the impact of radio luminous AGN on galaxy formation.

The paper is outlined as follows. In Sec. 2 we define the VLA-COSMOS AGN sample. In Sec. 3 we derive the radio luminosity function for the VLA-COSMOS AGN, and extend it to high radio powers using the results from Willott et al. (2001). In Sec. 4 we constrain the evolution of radio AGN out to $z = 1.3$. In Sec. 5 we analyze the properties of local and intermediate redshift weak and powerful radio AGN; in Sec. 6 we compute the radio AGN mass function, and derive and compare the star formation quenching and radio-AGN triggering rates. We discuss our results in the context of galaxy formation and evolution in Sec. 7, and summarize them in Sec. 8.

---

[17] A spectral index of $\alpha = 0.7$ ($F_\nu \propto \nu^{-\alpha}$; where F_ν is the radio flux density) is assumed throughout the paper.

We report magnitudes in the AB system, adopt $H_0 = 70, \Omega_M = 0.3, \Omega_\Lambda = 0.7$, and define the radio synchrotron spectrum as $F_\nu \propto \nu^{-\alpha}$, assuming $\alpha = 0.7$.

2. THE VLA-COSMOS RADIO AGN SAMPLE

The sample of AGN galaxies used here is presented in Smolčić et al. (2008a, S08a hereafter), and we briefly summarize it below.

Using radio and optical data for the COSMOS field, S08a have constructed a sample of 601 AGN galaxies with $z \leq 1.3$ from the entire VLA-COSMOS Large Project catalog (Schinnerer et al. 2007). The selection required optical counterparts with $i_\mathrm{AB} \leq 26$, accurate photometry, and a S/N ≥ 5 (i.e. $\gtrsim 50$ μJy) detection at 20 cm, and is based on a rest-frame optical color classification (see also Smolčić et al. 2006). The classification method was well-calibrated using a large local sample of galaxies ($\sim 7,000$ SDSS "main" spectroscopic galaxy sample, NVSSand IRAS surveys) representative of the VLA-COSMOS population. It was shown that the method agrees well with other independent classification schemes based on mid-infrared colors (Lacy et al. 2004; Stern et al. 2005) and optical spectroscopy (Baldwin, Phillips & Terlevich 1981; Best et al. 2005). The selected sample of AGN is estimated to be $\sim 90\%$ complete.

The rest-frame color classification procedure efficiently selects mostly type 2 AGN (such as LINER, Seyferts), and absorption-line AGN (with no emission lines in the optical spectrum), while type 1 AGN (i.e. quasars, $\lesssim 20\%$ of the total AGN sample) are not included in the current sample (see S08a for detailed definitions of the samples).

Although based on a color identification (as opposed to an optical spectroscopic classification), the output of the selection of our intermediate redshift ($z \leq 1.3$) AGN sample is comparable to those of numerous local ($z \leq 0.3$) radio AGN samples extensively studied in the literature (e.g. Sadler et al. 2002; Best et al. 2005; Mauch & Sadler 2007, drawn from the SDSS, 2dF, and 6dF optical surveys combined with the NVSS and FIRST 20 cm radio surveys). This is an important feature as it enables a straight-forward and fair comparison of our results with those based on these local studies (e.g. the local AGN radio luminosity function).

Out of the 601 selected AGN galaxies 262 have spectroscopic redshifts, while the remaining sources have very reliable photometric redshifts available ($\sigma\left(\frac{\Delta z}{1+z}\right) = 0.027$; see S08a and references therein). Based on Monte Carlo simulations, S08a have shown that the photometric errors in the rest-frame color introduce a small, $\sim 5\%$, uncertainty in the number of the selected galaxies. Here we use the S08a sample of AGN galaxies, statistically corrected for this effect.

3. THE 1.4 GHZ LUMINOSITY FUNCTION FOR RADIO AGN IN VLA-COSMOS

3.1. *Derivation of the luminosity function (LF)*

We derive the radio LF (Φ) for our AGN galaxies in four redshift bins using the standard $1/V_\mathrm{max}$ method (Schmidt 1968). We limit the accessible volumes a) on the bright end by the minimum redshift cut-off of the redshift range in consideration or the minimum redshift out to which an object could be observed due to the optical saturation limit of $i^* = 16$ (AB mag; see also Capak et al. 2007), and b) on the faint end by the maximum redshift out to which a galaxy could be observed given the flux limits on both the radio and optical data. In practice, the latter is dominated by the radio detection limits, rather than the optical, as the major fraction of the sources used here has i_AB band magnitudes brighter than ~ 24 (see Fig. 21 in S08a).

We further take into account the non-uniform rms noise level in the VLA-COSMOS mosaic via the differential visibility area (i.e. areal coverage, A_k, vs. rms; see Fig. 13 in Schinnerer et al. 2007). Hence, for a source with a 1.4 GHz luminosity L_j its maximum volume is $V_\mathrm{max}(L_j) = \sum_{k=1}^{n} A_k \cdot V_\mathrm{max}(z_\mathrm{max}^{A_k}, L_j)$.

In order to robustly derive the LF we take several additional corrections into account: a) the VLA-COSMOS detection completeness (Bondi et al. 2008), and b) the AGN galaxy selection bias due to the rest-frame color uncertainties. We correct for these in the same way as described in Smolčić et al. (2008b, S08b hereafter). The median of the first correction (as a function of flux density) is $\sim 10\%$ (reaching a maximum value of 60% in only one of the lowest flux density bins; see Tab. 1 in Bondi et al. 2008). The second correction, based on Monte Carlo simulations, yields a reduction of $\sim 5\%$ of the average number of radio AGN (see below; see also S08b for a more detailed description).

Hence, in the i$^\mathrm{th}$ luminosity bin the comoving space density (Φ_i), and its corresponding error (σ_i), are computed by weighting the contribution of each (j$^\mathrm{th}$) galaxy by the completeness correction factor, f_det (see Bondi et al. 2008):

$$\Phi_i = \sum_{j=1}^{N} \frac{\mathrm{f}_\mathrm{det}^\mathrm{j}}{\mathrm{V}_\mathrm{max}^\mathrm{j}} \; ; \quad \sigma_i = \sqrt{\sum_{j=1}^{N} \left(\frac{\mathrm{f}_\mathrm{det}^\mathrm{j}}{\mathrm{V}_\mathrm{max}^\mathrm{j}}\right)^2} \qquad (1)$$

The selection bias due to the rest-frame color uncertainties is accounted for via Monte Carlo simulations. As described in S08a and S08b, in each iteration the rest-frame color error distribution is generated (see Fig. 5 in S08a) and added to the rest-frame color derived by SED fitting. AGN galaxies are then re-selected, and the LF is derived as described above. In this way we obtain 100 realizations of (Φ_i,σ_i) for each luminosity bin, and we take the median values as representative.

3.2. *The radio AGN luminosity function*

The 1.4 GHz radio LFs for our AGN galaxies for the 4 chosen redshift bins are shown in Fig. 1, and tabulated in Tab. 1. In each panel in Fig. 1 we also show the local 20 cm LFs for AGN derived by Condon et al. (2002), Sadler et al. (2002), Best et al. (2005), and Mauch & Sadler (2007). Our derived LF in the local redshift bin (top left panel) agrees well with the local LFs. This is quite remarkable as a) our identification method is based only on photometry contrary to

TABLE 1
Luminosity functions for VLA-COSMOS AGN

redshift range	$L_{1.4\mathrm{GHz}}$ [WHz^{-1}]	Φ [Mpc^{-3}dex^{-1}]
$0.1 < z \leq 0.35$	$4.47 \cdot 10^{21}$	$5.08 \pm 2.25 \cdot 10^{-4}$
	$1.41 \cdot 10^{22}$	$2.54 \pm 0.66 \cdot 10^{-4}$
	$4.47 \cdot 10^{22}$	$2.22 \pm 0.40 \cdot 10^{-4}$
	$1.58 \cdot 10^{23}$	$4.54 \pm 1.57 \cdot 10^{-5}$
	$5.62 \cdot 10^{23}$	$1.21 \pm 0.70 \cdot 10^{-5}$
	$1.78 \cdot 10^{24}$	$1.66 \pm 0.88 \cdot 10^{-5}$
	$5.62 \cdot 10^{24}$	$7.90 \pm 5.59 \cdot 10^{-6}$
	$1.78 \cdot 10^{25}$	$1.46 \pm 0.84 \cdot 10^{-5}$
$0.35 < z \leq 0.6$	$3.16 \cdot 10^{22}$	$1.90 \pm 0.55 \cdot 10^{-4}$
	$7.94 \cdot 10^{22}$	$1.70 \pm 0.29 \cdot 10^{-4}$
	$2.00 \cdot 10^{23}$	$4.48 \pm 1.18 \cdot 10^{-5}$
	$5.62 \cdot 10^{23}$	$1.40 \pm 0.57 \cdot 10^{-5}$
	$1.41 \cdot 10^{24}$	$8.96 \pm 3.96 \cdot 10^{-6}$
	$3.16 \cdot 10^{24}$	$4.49 \pm 2.81 \cdot 10^{-6}$
	$7.94 \cdot 10^{24}$	$4.53 \pm 2.84 \cdot 10^{-6}$
$0.6 < z \leq 0.9$	$1.00 \cdot 10^{23}$	$8.76 \pm 2.32 \cdot 10^{-5}$
	$2.51 \cdot 10^{23}$	$8.75 \pm 1.36 \cdot 10^{-5}$
	$6.31 \cdot 10^{23}$	$2.86 \pm 0.61 \cdot 10^{-5}$
	$1.78 \cdot 10^{24}$	$2.45 \pm 0.50 \cdot 10^{-5}$
	$4.47 \cdot 10^{24}$	$4.11 \pm 1.82 \cdot 10^{-6}$
	$1.00 \cdot 10^{25}$	$3.43 \pm 1.66 \cdot 10^{-6}$
	$2.24 \cdot 10^{25}$	$6.88 \pm 7.45 \cdot 10^{-7}$
$0.9 < z \leq 1.3$	$3.16 \cdot 10^{23}$	$3.72 \pm 0.93 \cdot 10^{-5}$
	$7.08 \cdot 10^{23}$	$2.28 \pm 0.47 \cdot 10^{-5}$
	$1.78 \cdot 10^{24}$	$1.82 \pm 0.34 \cdot 10^{-5}$
	$5.01 \cdot 10^{24}$	$3.97 \pm 1.38 \cdot 10^{-6}$
	$1.26 \cdot 10^{25}$	$4.25 \pm 1.33 \cdot 10^{-6}$
	$3.16 \cdot 10^{25}$	$1.42 \pm 0.77 \cdot 10^{-6}$
	$7.08 \cdot 10^{25}$	$7.16 \pm 5.48 \cdot 10^{-7}$
	$1.78 \cdot 10^{26}$	$1.46 \pm 0.79 \cdot 10^{-6}$

· $H_0 = 70$, $\Omega_M = 0.3, \Omega_\Lambda = 0.7$

the spectroscopic selection performed by the other studies (Sadler et al. 2002; Best et al. 2005; Mauch & Sadler 2007), and b) the 2□° COSMOS field samples a significantly smaller comoving volume at these low redshifts compared to the almost all-sky surveys used by the other studies. This verifies that both our selection method, as well as the derivation of the LF are correct. Within the errors our lowest-redshift LF seems to be best represented by the local LF derived by Sadler et al. (2002, Sad02 hereafter), and we adopt this local LF for further analysis of the evolution of our AGN population.

In the top right panel in Fig. 1 we compare our derived AGN LF ($0.35 < z \leq 0.6$) with the volume densities computed by Sadler et al. (2007) for a redshift range $0.4 < z < 0.7$ based on 2SLAQ Luminous Red Galaxy Survey and NVSS, FIRST data. We convert their data to a base of $d\log L$, and scale them to match the mean redshift of our redshift bin ($z = 0.475$ compared to their $z = 0.55$) using pure luminosity evolution as obtained by Sadler et al. (2007, note that this only decreases their radio luminosities by 10%). The LFs are in excellent agreement. It is noteworthy that we well constrain the volume densities at the low luminosity end ($\lesssim 10^{25}$ W Hz^{-1}), while the sample of Sadler et al. (2007) extends further out to 1.6×10^{27} W Hz^{-1} (see also Fig. 3, and Sec. 7).

The VLA-COSMOS AGN volume densities in the two highest redshift bins ($0.6 < z \leq 0.9$ and $0.9 < z \leq 1.3$) are shown in the bottom panels in Fig. 1. The radio AGN LF at these redshifts has been studied in full detail only for higher power AGN ($L_{1.4\mathrm{GHz}} > 10^{25}$ W Hz^{-1}; Dunlop & Peacock 1990; Willott et al. 2001; Waddington et al. 2001), while constraining the low-luminosity end (sampled here) has been hampered by low number statistics due to small field sizes. Cowie et al. (2004) combined two deep 1.4 GHz radio surveys of the HDF-N (40′ in diameter; $5\sigma \sim 40$ μJy in the central region) and SSA13 (34′ in diameter; $5\sigma \sim 25$ μJy in the center) fields, and derived the AGN radio LF in two separate redshift ranges similar to ours, and at comparable luminosities to our work. Our results are in qualitative agreement with those derived by Cowie et al. (2004, c.f. their Fig. 3). However, their sample is a factor of ~ 7 smaller than the one used here.

4. THE EVOLUTION OF RADIO AGN

In this section we constrain the evolution of our low-power radio AGN using the VLA-COSMOS AGN data (Sec. 4.1). We further extend this to high-power radio AGN using the model obtained by Willott et al. (2001) based on high-power AGN samples drawn from the 3CRR, 6CE, and 7CRS surveys (Sec. 4.2).

4.1. *The evolution of low-power radio AGN galaxies in the COSMOS field*

The evolution of an astrophysical population is usually parameterized by monotonic density and luminosity evolution of its local luminosity function:

$$\Phi_z(L) = (1+z)^{\alpha_D} \times \Phi_{z=0}\left[\frac{L}{(1+z)^{\alpha_L}}\right] \qquad (2)$$

where α_D and α_L are the characteristic density and luminosity evolution parameters, respectively, L is the luminosity, $\Phi_z(L)$ is the luminosity function at redshift z, and $\Phi_{z=0}$ is the local luminosity function.

It is well known that strong degeneracy between luminosity and density evolution exists, even if the observational data sample the turn-over ('knee') of the LF at different cosmological times (see e.g. Le Floc'h et al. 2005). The VLA-COSMOS AGN sample in particular lacks high luminosity objects that could constrain the turn-over of the LF in all our redshift bins (see Fig. 1). Hence, we do not attempt to try to break the luminosity – density evolution degeneracy, but we separately constrain both pure density (PDE; $\alpha_L = 0$) and pure luminosity (PLE; $\alpha_D = 0$) evolution based on our data. We adopt the Sad02 local AGN LF ($\Phi_{z=0}$) as the representative LF in the local universe, which is given by the following analytical form:

$$\Phi(L) = \Phi^* \left[\frac{L}{L_*}\right]^{1-\alpha} \exp\left\{-\frac{1}{2\sigma^2}\left[\log\left(1+\frac{L}{L_*}\right)\right]^2\right\} \qquad (3)$$

where $\alpha = 1.58$, $\sigma = 1.0$, $\Phi^* = 7.6 \times 10^{-6}$ Mpc^{-3}, and $L^* = 2.1 \times 10^{24}$ W Hz^{-1} for their AGN population (scaled to the cosmology used here, and to the base of $d\log L$).

For both PDE and PLE we derive the evolution by summing the χ^2 distributions obtained for a large range of evolution parameters α_L and α_D [(α_L,0) for PLE; (0,α_D) for PDE] in each particular redshift bin (excluding our first – local – redshift bin). The uncertainty in α is then taken to be the 1σ error obtained from the

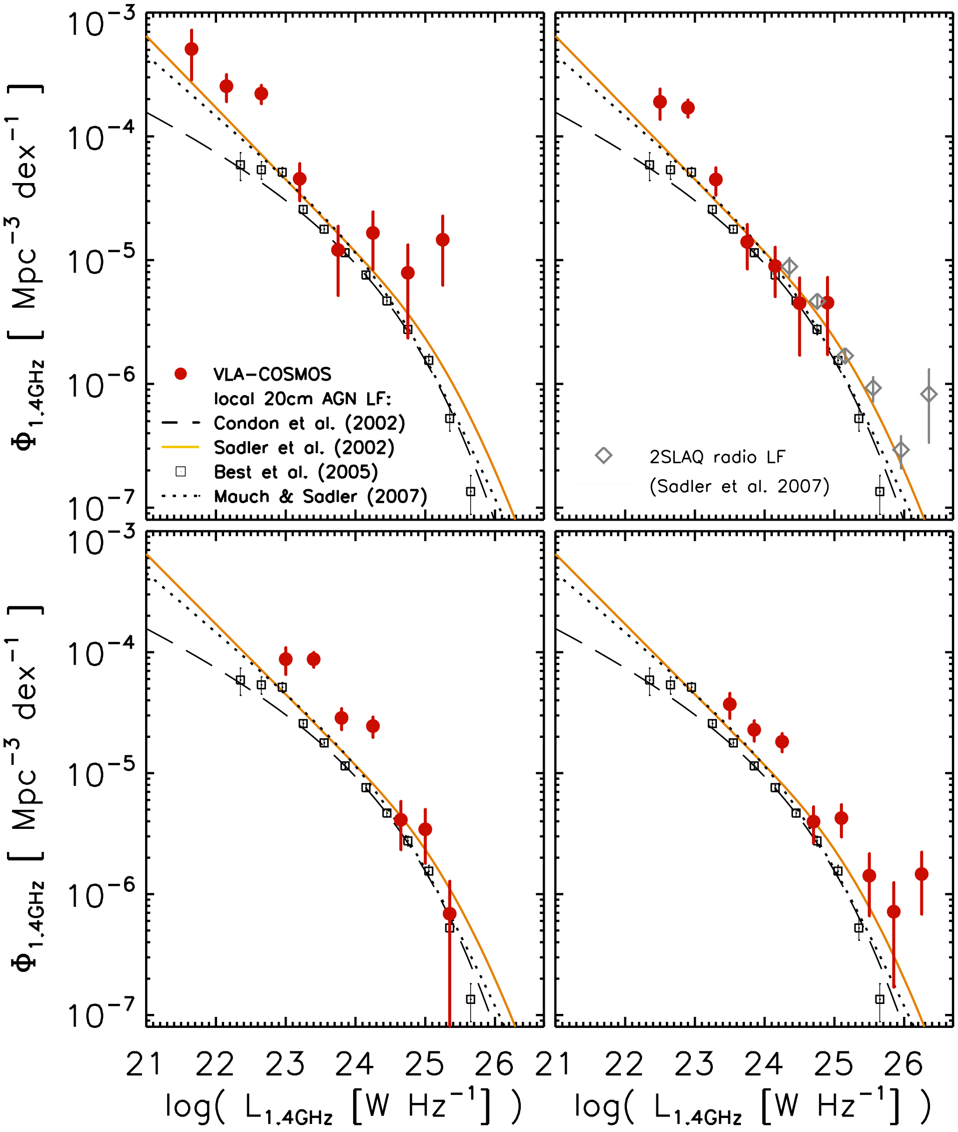

FIG. 1.— 1.4 GHz luminosity functions (LFs) for AGN in the VLA-COSMOS survey (filled red circles), shown for four redshift ranges indicated in each panel. The local AGN volume densities derived by Condon et al. (2002, dashed black line), Sadler et al. (2002, solid orange line), Best et al. (2005, empty squares), and Mauch & Sadler (2007, dotted line) are also plotted in each panel. The empty symbols in the top right panel are the radio AGN volume densities derived for the redshift range $0.4 < z < 0.7$ by Sadler et al. (2007) for the 2SLAQ Luminous Red Galaxy survey sample, and scaled here to match our mean redshift value of 0.475 (see text for details).

χ^2 statistics. Our results yield a pure density evolution with $\alpha_D = 1.1 \pm 0.1$, or alternatively a pure luminosity evolution with $\alpha_L = 0.8 \pm 0.1$.

In Fig. 2 we show the luminosity density for our AGN in the four redshift ranges defined in Fig. 1. We also plot the luminosity density given the derived PD and PL evolutions (lines). From the figure it becomes obvious that we cannot distinguish between these two types of evolution given our data, as our sample, tracing only the lower luminosity end of the luminosity function, appears to be described equally well by both. Thus, in the further analysis we will take the range of the two best fit evolution models (taking also their errors into account) as representative of the range of uncertainties.

In summary, our results imply either a pure luminosity evolution with $L_* \propto (1+z)^{0.8\pm0.1}$ or a pure density evolution where $\Phi_* \propto (1+z)^{1.1\pm0.1}$. Regardless of which model is physically more appropriate to describe the real cosmic evolution of the VLA-COSMOS AGN population, both imply a modest evolution of radio luminous AGN in the luminosity range of $\sim 10^{22-25}$ W Hz^{-1}.

Our results are consistent with previous findings. Based on a $V/V_{\rm max}$ analysis out to a redshift of ~ 1, Clewley & Jarvis (2004) have found no strong evolution of low radio luminosity sources ($L_{\rm 325MHz} \lesssim 10^{25}$ W Hz^{-1} sr^{-1}, corresponding to $L_{\rm 1.4GHz} \lesssim 4.5 \times 10^{25}$ W Hz^{-1}) at least up to $z \sim 0.6$. Further, Sadler et al. (2007) have constrained the evolution of the luminosity function for radio luminous AGN ($L_{\rm 1.4GHz} \sim 10^{24-27}$ W Hz^{-1}) out to $z \sim 0.7$. Using the local AGN

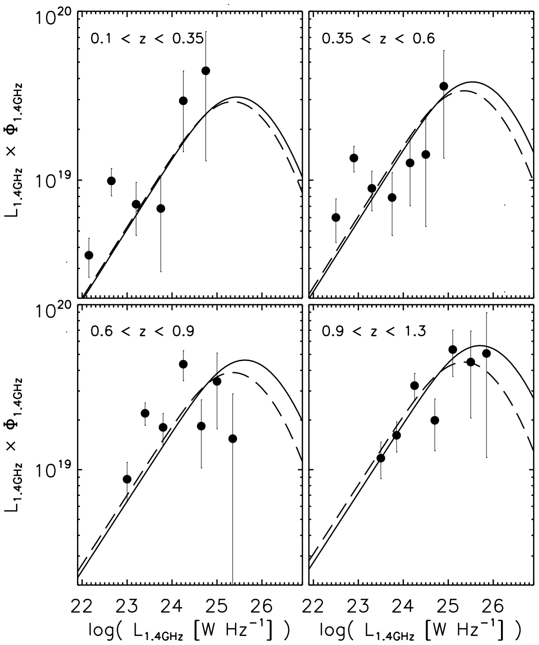

Fig. 2.— Luminosity density for the VLA-COSMOS AGN in four redshift ranges (filled circles). The lines represent the best fit pure density (dashed line) and pure luminosity (solid line) evolution of the local 20 cm AGN luminosity function (see text for details).

LF given by Mauch & Sadler (2007) they have found a pure luminosity evolution with $L_* \propto (1+z)^{2.0\pm0.3}$. The VLA-COSMOS AGN LF in the redshift range $0.35 < z \leq 0.6$, and the Sadler et al. (2007) AGN LF ($0.4 < z < 0.7$) agree remarkably well (see top right panel in Fig. 1 & Fig. 3). If we parameterize the evolution of the VLA-COSMOS AGN in the same way as described in Sadler et al. (2007, using the same local LF), we derive a pure luminosity evolution of 1.2 ± 0.4 for the $0.35 < z \leq 0.6$ redshift bin. It has to be noted, however, that the VLA-COSMOS and the 2SLAQ samples constrain different radio luminosity ranges (see Fig. 3). Our results agree within the uncertainties with those of Mauch & Sadler (2007), however they on average imply a slower evolution. This is consistent with a more modest evolution of low radio-power, compared to high radio-power, radio AGN (Willott et al. 2001; Waddington et al. 2001; Clewley & Jarvis 2004). Our findings are also in very good agreement with the recent results based on NVSS/FIRST and the MegaZ-Luminous Red Galaxy catalog drawn from the SDSS (Donoso et al. 2008).

4.2. *The evolution of high-power radio AGN*

In order to quantify the contribution of different populations to the comoving radio energy density at different cosmic times, *all* radio AGN populations need to be considered. As low- and high- power radio AGN seem to evolve in a different manner (see Sec. 1) and our VLA-COSMOS AGN sample only the low power radio AGN, we need to make the following assumptions about the evolution of the high power radio sources.

Based on the 3CRR, 6CE, and 7CRS radio surveys combined with complete optical spectroscopy, Willott et al. (2001) have successfully modeled the radio AGN LF using two radio populations – a less powerful ($L_{1.4GHz} \sim 2.5 \times 10^{25-27}$ W Hz^{-1}) population comprising both FR I and FR II sources, and a powerful population ($L_{1.4GHz} \gtrsim 2.5 \times 10^{26}$ W Hz^{-1}) comprising mostly FR II sources. They have modeled the evolution of the first population as a pure density evolution up to a maximum redshift (~ 0.7) beyond which any evolution ceases. The evolution of the powerful population has been assumed to change in density following a Gaussian distribution in redshift, which was allowed to have a different shape beyond its redshift peak at $z \sim 2$ (see Tab. 1 in Willott et al. 2001). It is worth noting that the Willott et al. model agrees well with the Dunlop & Peacock (1990) steep spectrum model.

The VLA-COSMOS AGN sample constrains the faint end of the radio AGN luminosity function, and here we use the Willott et al. (2001) model to extend our radio LF to high powers. In Fig. 3 we compare our LFs with the Willott et al. (2001) model, after the latter has been converted to the current cosmology and the 151 MHz radio luminosities scaled to 1.4 GHz. The VLA-COSMOS AGN data and the Sad02 LF constrain the radio LF more robustly at the faint end compared to the Willott et al. (2001) model for their *less-powerful radio AGN*. Thus, in the further analysis we will constrain the low-power radio AGN LF and its evolution using the VLA-COSMOS sample as described in the previous section, and we will use *only* the powerful radio AGN model by Willott et al. (2001) to describe the evolution of high radio-power AGN (see dash-dotted curves in Fig. 3).

4.3. *The evolution of the comoving radio luminosity density for AGN galaxies*

At a specific cosmic time the integrated comoving luminosity density represents the total power per unit comoving volume of a given astronomical population. Thus, if divided into distinct populations of objects it traces their relative contribution to the overall power output at a given redshift. To estimate the contribution of low and high radio power AGN to the AGN radio luminosity output at different cosmic times, we investigate in the following the evolution of the comoving 1.4 GHz luminosity density, $\Omega_{1.4GHz}$, for our VLA-COSMOS AGN ($L_{1.4GHz} \lesssim 10^{25}$ W Hz^{-1}) and the high-power AGN ($L_{1.4GHz} \gtrsim 10^{26}$ W Hz^{-1}), adopting the Willott et al. (2001) model.

For a given redshift $\Omega_{1.4GHz}$ has been computed by integrating the luminosity density over the entire range of radio luminosities. For the VLA-COSMOS AGN the luminosity density has been constrained using our best fit PLE and PDE models (see curves in Fig. 2 and Sec. 4.1), and for the high-power population using the Willott et al. (2001) model 'C', with the corresponding errors (see tab. 1 in Willott et al. 2001 and Sec. 4.2).

In Fig. 4 we show the evolution of the comoving 20 cm integrated luminosity density for all radio AGN as well as the low and high radio power AGN separately. The evolution of these two populations is very different; high-power AGN evolve significantly stronger than low-power AGN. The total $\Omega_{1.4GHz}$ for radio AGN is dominated by low-power AGN at low redshifts ($z \lesssim 0.7$) where the contribution of high-power radio sources is negligible. However, at $z \gtrsim 0.7$ high-power sources begin to contribute significantly to the overall integrated luminosity

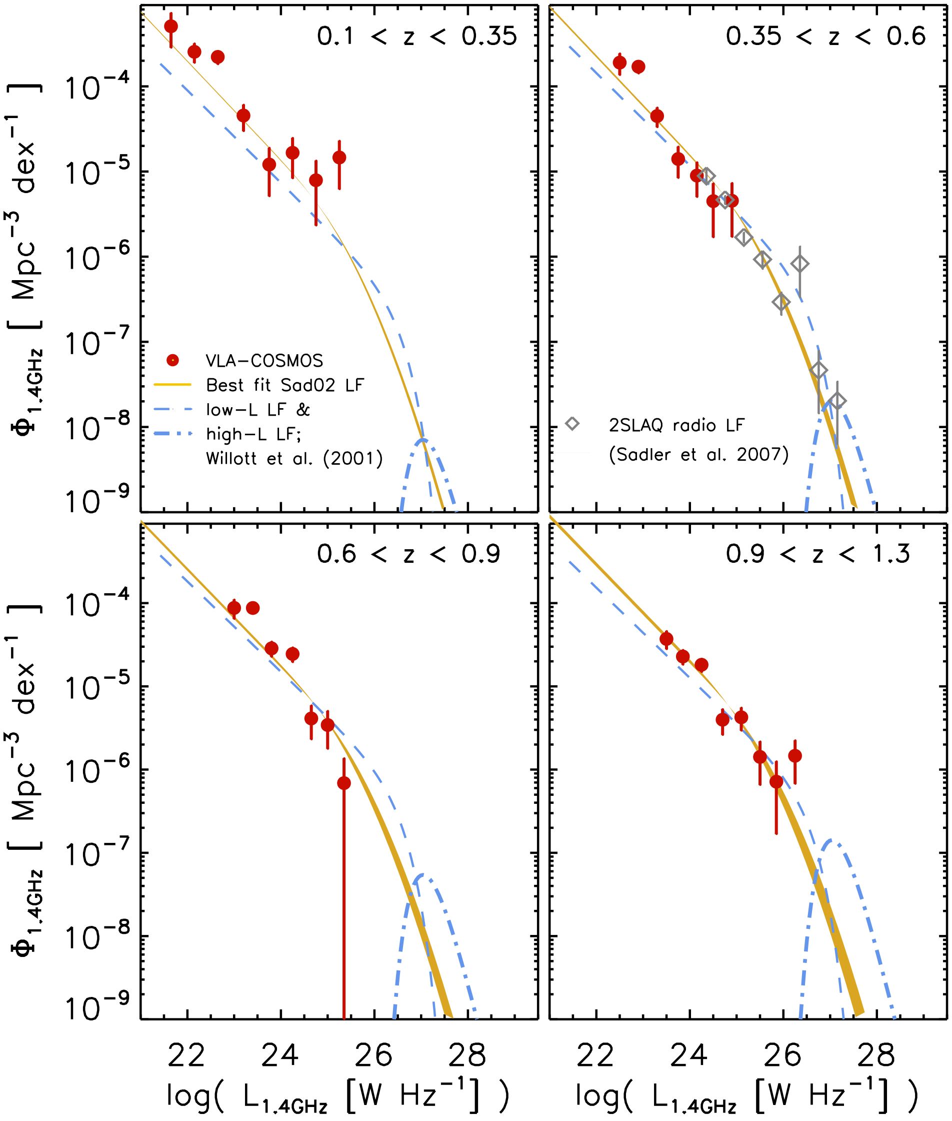

FIG. 3.— VLA-COSMOS AGN volume densities at 20 cm in four redshift ranges (red filled circles; analogous to Fig. 1). Also shown in each panel is our best fit evolution corresponding to the range given by pure density and pure luminosity evolution of the Sad02 local LF and their corresponding errors (orange shaded curve), as well as the radio AGN luminosity function model given by Willott et al. (2001, model 'C') for their less luminous population (dashed blue curves), and high-luminosity population (dash-dotted blue curves; scaled to current cosmology and 1.4 GHz radio frequency; see text for details). In the top right panel the volume densities derived by Sadler et al. (2007, scaled to match our mean redshift value of 0.475; see also Fig. 1) are shown.

density, and at a redshift of ~ 1.3 their contribution to the total AGN $\Omega_{1.4\mathrm{GHz}}$ is comparable to the one of low-power AGN. The implications of these populations for galaxy formation and evolution, also out to higher redshifts ($z = 2.5$), are discussed in Sec. 7.

5. PROPERTIES OF RADIO AGN

In this section we outline and compare the properties of low and high radio-power AGN in the local (Sec. 5.1) and intermediate-redshift (Sec. 5.2) universe. We find that already by $z \sim 1$ the host galaxies of low-power, VLA-COSMOS AGN have built-up stellar and black hole masses comparable to the highest mass galaxies observed locally. As their black hole masses are already significant at these intermediate redshifts, this implies that they will no longer be able to have a phase of high accretion (i.e. vigorous BH growth), consistent with numerous previous studies of similar samples (e.g. Allen et al. 2006; Evans et al. 2006; Hardcastle et al. 2006, 2007). For the high radio power AGN on the other hand, extensive evidence exists in the literature that they accrete at high rates – representing a mode of substantial BH growth.

5.1. *Local universe*

Various correlations are found in the literature between the presence of emission lines in AGN and their e.g. radio power, black hole and stellar mass, as well as environment and the galaxies' gas content. We outline these below.

First, almost all FR I – low power – radio galaxies are

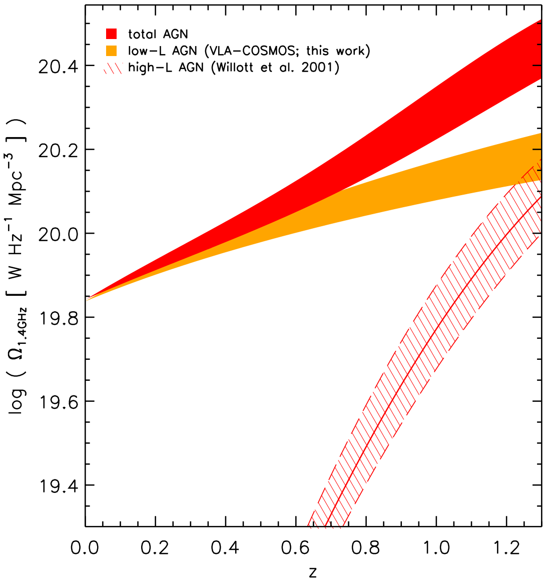

FIG. 4.— Evolution of the comoving 20 cm integrated luminosity density for VLA-COSMOS AGN (orange curve) galaxies since $z = 1.3$. Shown is also the evolution of the high-luminosity radio AGN, adopted from Willott et al. (2001, hatched region; the thick and dashed lines correspond to the mean, maximum and minimum results, respectively). The evolution for the total AGN population, obtained by co-adding the VLA-COSMOS and high-luminosity AGN energy densities, is shown as the red-shaded curve (see text for details).

LERAGN, while optical hosts of FR IIs, which are typically more powerful than FR Is (Fanaroff & Riley 1974; Owen 1993; Ledlow & Owen 1996), usually have strong emission lines[18]. Recently, based on a large statistically significant sample of local radio - optical sources (SDSS-NVSS-FIRST) Kauffmann et al. (2008) have found that the fraction of radio AGN whose optical hosts have emission lines in their spectra (predominantly HERAGN) is a strong function of radio luminosity. This emission-line galaxy fraction is roughly constant ($\sim 40\%$) up to $L_{1.4GHz} \sim 10^{25}$ W Hz^{-1}, beyond which it steeply rises approaching $\sim 80\%$ at $\sim 4 \times 10^{25}$ W Hz^{-1} (see Fig. 3 in Kauffmann et al. 2008). This 'critical' luminosity, observed by Kauffmann et al., is remarkably close to the FR I – II break luminosity, as well as to the power which roughly separates the radio sources which show strong cosmological evolution from those which do not (see e.g. Fig. 4 and Sec. 4). Furthermore, based on the results of Kauffmann et al., *the luminosity of* $L_{1.4GHz} \sim 10^{25}$ *W Hz*$^{-1}$ *can be thought of as a rough threshold between high- and low- excitation radio AGN.* Thus, most of the low radio power AGN ($L_{1.4GHz} \lesssim 10^{25}$ W Hz^{-1}) are LERAGN, while the majority of powerful radio AGN ($L_{1.4GHz} \gtrsim 10^{25}$ W Hz^{-1}) are HERAGN.

On the other hand, the fraction of emission line (i.e. high-excitation) radio AGN in the local universe strongly *decreases* as a function of both stellar mass and velocity dispersion (see Fig. 3 in Kauffmann et al. 2008). This implies that, at least locally, high-excitation (or alternatively high radio power) AGN tend to have lower stellar masses, as well as lower black hole masses compared to LERAGN. Even further, the latter constitute the most massive galaxies in the universe ($M_\odot > 10^{11}$ M$_\odot$) that preferentially occupy the centers of high galaxy density regions (Baum et al. 1992, Best et al. 2005).

Furthermore, various studies in the literature have shown that HERAGN, contrary to LERAGN, tend to show unusually blue off-nuclear continuum colors (Baum et al. 1992), evidence of recent star formation (Baldi & Capetti 2008), and often have distorted optical morphologies suggesting that they have undergone a recent major merger (Heckman et al. 1986; Baum et al. 1992; Baldi & Capetti 2008). CO and HI observations of radio galaxies suggest larger amounts of cold gas in powerful, compared to low-power, radio sources (see e.g. Fig. 8 in Evans et al. 2005, see also Emonts et al. 2008), and there is evidence supporting quantitatively larger amounts of dust, and therefore gas (Leon et al. 2001; Solomon & Vanden Bout 2005) in HERAGN compared to LERAGN (de Koff et al. 2000, Müller et al. 2004). A summary of the properties of radio AGN in the nearby universe is given in Tab. 2.

5.2. *Intermediate redshift*

In this section we investigate the properties of low and high radio-power AGN at intermediate redshifts, and compare these to the properties of their local counterparts. In Sec. 3 and Sec. 4 we have derived the 1.4 GHz radio luminosity function, and its evolution, for a sample of $\sim$ 600 radio luminous AGN ($0.1 < z < 1.3$) drawn from the VLA-COSMOS survey. One of the main characteristics of this radio AGN sample is that it consists of predominantly (96%) low-power AGN with $L_{1.4GHz} \lesssim 10^{25}$ W Hz^{-1}. Ledlow & Owen (1996) have shown that the threshold between weak FR I types of galaxies and powerful FR IIs is a function of the host galaxy's optical (R band) magnitude, M_R. Hence, to better constrain the properties of the VLA-COSMOS AGN in Fig. 5 we plot them in the $L_{1.4GHz}$ vs. M_R plane. Almost all (98%) of our AGN occupy the weak radio AGN, FR I region in this plane.

In order to get a further insight into the composition of the VLA-COSMOS AGN, we make use of the sources with available optical spectroscopy. Trump et al. (2007) have carried out a spectroscopic survey of X-ray and radio selected AGN candidates in the COSMOS field (using the Magellan/IMACS instrument). They have classified their sources into a) broad emission line AGN ('bl'), b) narrow emission line AGN ('nl'), c) red galaxies with only absorption features in their spectrum ('e') and d) hybrid objects showing a mix of narrow emission lines and a red galaxy continuum shape ('nle'). Combining a radio AGN detection with this classification scheme, we can very roughly consider the red and hybrid galaxy spectroscopic classification ('e'+'nle') as a proxy for LERAGN, and the narrow emission line AGN classification ('nl') as a proxy for HERAGN. About 35% of our VLA-COSMOS AGN have an available classification based on IMACS spectroscopy, and in Fig. 6 the fractions of 'e+nle' and 'nl' galaxies are shown as a function of both redshift (left panel) and radio luminosity (right panel). The absorption line and hybrid galaxies dominate the VLA-COSMOS sample at a constant $\sim 80\%$ level at all redshifts ($z \leq 1.3$), while the narrow emission line AGN

---

[18] Note, however, that the correspondence between the FR class and the presence of emission lines is not exactly one-to-one.

TABLE 2
Properties of LERAGN and HERAGN in the local universe

Property	LERAGN	Ref.	HERAGN	Ref.
Object class	mainly FR I	(1),(2)	mainly FR II	(1),(2)
radio luminosity	$L_{1.4\mathrm{GHz}} \lesssim 10^{25}$ W Hz^{-1}	(3)	$L_{1.4\mathrm{GHz}} \gtrsim 10^{25}$ W Hz^{-1}	(3)
density environment	moderate-to-high	(4),(5)	moderate-to-low	(4)
optical morphology	regular	(8),(9)	often distorted	(8),(9),(10)
optical color	red	(9),(11)	bluer (compared to LERAGN)	(10),(9)
stellar mass	highest ($\gtrsim 5 \times 10^{10}$ M$_\odot$)	(3),(11)	lower (compared to LERAGN)	(3),(12)
BH mass	highest ($\sim 10^9$ M$_\odot$)	(9),(13)	lower (compared to LERAGN)	(3),(14)
ISM content	low	(15),(16),(17)	higher (compared to LERAGN)	(15),(16),(17),(18),(19)
accretion mode	radiatively inefficient	(1),(2),(14),(20)	radiatively efficient	(1),(2),(20),(21),(22)

Note. — References: (1) Evans et al. 2006, (2) Hardcastle et al. 2006, (3) Kauffmann et al. 2008, (4) Baum et al. 1992, (5) Best et al. 2005, (8) Heckman et al. 1986, (9) Baum et al. 1992, (10) Baldi & Capetti 2008, (11) Smolčić et al. 2008a, (12) Tasse et al. 2008, (13) this work, (14) Chiaberge et al. 2005, (15) Leon et al. 2001, (16) de Koff et al. 1996, (17) Müller et al. 2004, (18) Evans et al. 2006, (19) Emonts et al. 2008, (20) Hardcastle et al. 2007, (21) Barthel 1989, (22) Haas 2004

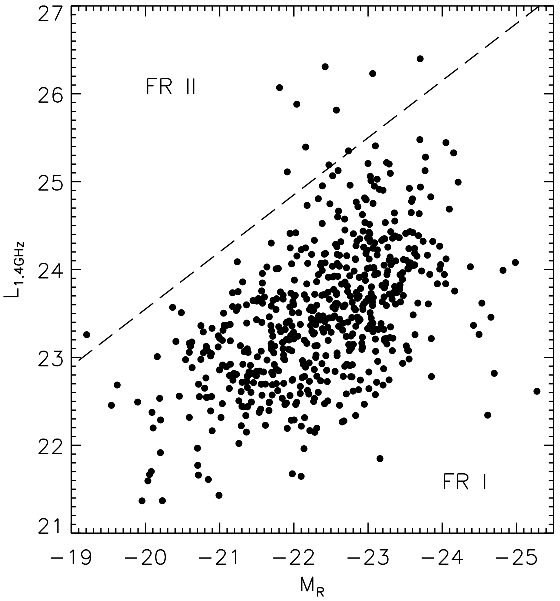

Fig. 5.— Monochromatic 1.4 GHz radio power for VLA-COSMOS AGN as a function of their host galaxy absolute R band magnitude. The dashed line corresponds to the separation between FR I and FR II types of galaxies given by Ledlow & Owen (1996). Note that almost all of the VLA-COSMOS AGN occupy the low-power FR I region of this plane.

contribute about $\sim 20\%$ at all redshifts. There is an indication that in the highest redshift bin ($1 < z < 1.3$), where our most luminous ($L_{1.4\mathrm{GHz}} > 10^{25}$ W Hz^{-1}) radio AGN are observed (see Fig. 1), the fraction of narrow emission line AGN rises. However, given the large errorbars in this redshift range (due to the low number of spectroscopically observed radio AGN) we cannot draw any robust conclusions regarding this. In the right panel of Fig. 6 we show the fraction of 'e+nle' and 'nl' galaxies as a function of 1.4 GHz power. Although the number of sources with $L_{1.4\mathrm{GHz}} \gtrsim 10^{25}$ W Hz^{-1} is low in the VLA-COSMOS AGN sample, there is an indication that the fraction of narrow-line objects (thus roughly HERAGN) increases beyond $\sim 10^{25}$ W Hz^{-1}, consistent with the findings in the local universe (Kauffmann et al. 2008).

Assuming that the spectroscopic sub-sample represents well the full sample (note that this is a rather robust assumption as shown in S08a; see their Figs. 3 and 21), we conclude that LERAGN dominate the VLA-COSMOS radio AGN sample. Thus, similar to the findings in the local universe, our low radio power AGN at intermediate redshift are preferentially LERAGN.

Stellar masses, using a Chabrier (2003) initial mass function (IMF), have been computed for the entire VLA-COSMOS galaxy sample ($z \leq 1.3$) by S08a. In Fig. 7 (top panels) we show the stellar masses for our VLA-COSMOS AGN as a function of redshift and 1.4 GHz luminosity. The median stellar mass of our radio AGN is 1.6×10^{11} M$_\odot$, i.e. $< \log M_* >= 11.2$ (in any given redshift range) with a 1σ scatter of 0.4 dex. This is consistent with the stellar masses of the most massive, local galaxies (e.g. Baldry et al. 2004; Best et al. 2005). In addition, it is worth noting that their average rest-frame colors are consistent with red galaxy colors (see e.g. Fig. 9 in S08a).

We further compute the BH masses for the full VLA-COSMOS AGN sample using the local correlation given by Marconi & Hunt (2003) which relates the K-band luminosity to the BH mass:

$$\log_{10} M_{\mathrm{BH}} = 8.21 + 1.13 \times (\log_{10} L_K - 10.9) \qquad (4)$$

L_K the rest-frame K-band luminosity (also in solar units). The scatter in the relation is 0.5 dex (Marconi & Hunt 2003). The K-band rest-frame luminosity for our VLA-COSMOS AGN was computed via SED fitting as described in detail in S08a. In order to take into account passive luminosity evolution (see Hopkins et al. 2006b and references therein) we change the normalization constant of the above relation as a function of redshift following the results from Hopkins et al. (2006b, see short-dashed line in the bottom left panel in their Fig. 2). In Fig. 7 (bottom panels) we plot the estimated BH masses as a function of both redshift and radio 1.4 GHz luminosity. The median BH mass of our radio AGN is $\log_{10} M_{\mathrm{BH}} = 8.8$ with a standard deviation of 0.4. Note that the apparent trend of BH mass with radio luminosity (bottom right panel in Fig. 7) reflects the dependence of radio luminosity on redshift in our radio flux limited sample (see Fig. 16 in S08a) rather than a real trend.

The black hole masses of our intermediate redshift radio AGN are comparable to the highest black hole masses known in the local universe (see e.g. McLure & Dunlop 2002, 2004). This implies that the low-power radio AGN have assembled their BH masses already by these intermediate redshifts, and that their BHs cannot grow

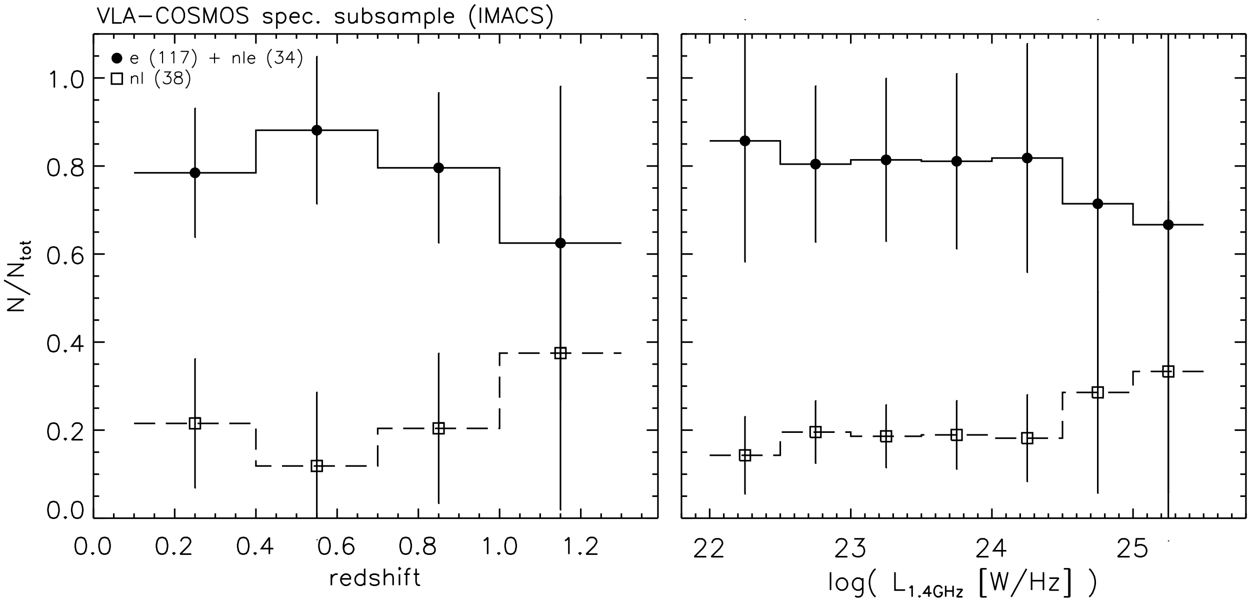

FIG. 6.— The fraction of VLA-COSMOS AGN with available Magellan/IMACS spectroscopy (Trump et al. 2007) as a function of redshift (left panel) and 1.4 GHz radio luminosity (right panel). The galaxies have been divided into two sub-samples, i) narrow emission line (nl) galaxies, and ii) elliptical galaxies (e) plus composite objects showing a red galaxy continuum and narrow emission lines (nle; see Trump et al. 2007 for details). These two subsamples roughly correspond to high- and low-excitation AGN, respectively (see text for details). The quantity and symbols for objects of each type is indicated in the left panel. Note that there is a slight (although noisy) trend showing that the fraction of narrow emission line objects (i.e. roughly high-excitation AGN) increases as a function of both redshift and radio luminosity.

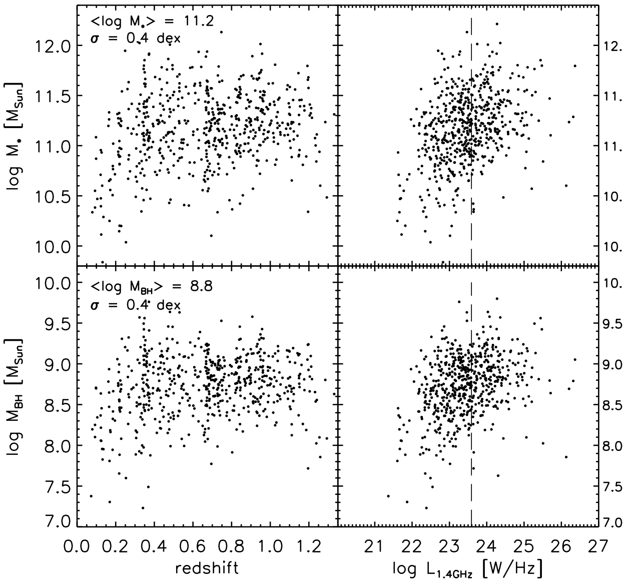

FIG. 7.— Logarithm of stellar (top panels) and black hole (bottom panels) masses for the VLA-COSMOS AGN as a function of redshift (left panels) and 1.4 GHz radio luminosity (right panels). The stellar masses were computed via SED fitting using the Bruzual & Charlot (2003) stellar population synthesis models (Chabrier 2003 IMF; see S08a for full details). The BH masses were derived using eq. 4, and corrected for passive luminosity evolution (see text for details). The dashed line in the right column corresponds to the lowest 1.4 GHz luminosity observable out to $z = 1.3$ given the VLA-COSMOS Large Project detection limit of ~ 50 μJy beam^{-1}.

significantly since $z \sim 1.3$. Therefore, they must be in a mode of modest growth in BH mass. This result is in agreement with numerous findings in the literature implying that LERAGN accrete radiatively inefficiently, at sub-Eddington rates (Allen et al. 2006; Evans et al. 2006; Hardcastle et al. 2006, 2007).

Given all of the above, the composition of our VLA-COSMOS AGN, the majority of which are shown to be LERAGN, is consistent with the properties of low radio-power AGN in the local universe: Our intermediate redshift AGN have already by $z \sim 1$ assembled both their stellar and black hole masses, comparable to the high-mass end of the galaxies known today.

On the other hand, powerful radio galaxies at high redshifts tend to show strong emission lines in their optical spectra (Rawlings et al. 1989, Baum & Heckman 1989, Rawlings & Saunders 1991; Willott et al. 1999, 2000), and are often associated with ongoing star-formation (Archibald et al. 2001, Greve et al. 2006, Seymour et al. 2008) as suggested by their bluer rest-frame colors (compared to red-sequence galaxies). Again, this is consistent with local observations of such sources. In numerous studies in the literature (e.g. Barthel 1989; Haas et al. 2004) these objects have been shown to accrete radiatively efficiently at high (∼ Eddington) accretion rates. Thus these HERAGN present a mode of significant BH growth – unlike the low radio power LERAGN.

To summarize, the properties of local and intermediate-redshift radio AGN, as shown above, suggest that radio activity is triggered in similar populations of objects independent of their redshift, i.e. cosmic time. This is in agreement with the finding that the rest-frame optical colors of radio source host galaxies do not change with redshift (Barger et al. 2007, S08a, Huynh et al. 2008). In addition, there is converging evidence that low radio power AGN reflect a modest – radiatively inefficient – mode of BH growth, while high radio power AGN are undergoing a phase of significant

– radiatively efficient – BH growth.

6. THE STAR FORMATION QUENCHING AND RADIO-AGN TRIGGERING RATES

One of the aims of this work is to study the link between radio AGN activity and star formation from an observational perspective. Thus, in order to investigate whether the processes responsible for the build up of the red galaxy sequence and the triggering of radio AGN mode are related or not, in this section we study the stellar mass properties of the red parent (Sec. 6.1) and radio AGN samples (Sec. 6.2), and derive and compare the rates for the star formation quenching (Sec. 6.3) and (low radio power) AGN triggering (Sec. 6.4). We find no evidence that these two processes are related. This however does not exclude the possibility that the radio AGN phase may be responsible for preventing already assembled massive galaxies to grow higher in mass, as explored in Sec. 7.3.

6.1. *The parent galaxy sample*

In order to derive the rates for star formation quenching and radio-AGN triggering we need to define a control-parent galaxy sample of our VLA-COSMOS radio AGN. We define this sample using the COSMOS photometric redshift catalog (Ilbert et al. 2008) from which we select galaxies with the same optical magnitude, redshift and color criteria applied to our VLA-COSMOS AGN (see Sec. 2). The rest-frame optical color P1 (constrained from the 3200 – 5800 Å range), which was used to select our VLA-COSMOS AGN is not available for the galaxies in the COSMOS photometric redshift catalog. Nonetheless, as the NUV-NIR galaxy SED has been shown to be a one-parameter family (e.g. Obrić et al. 2006; Smolčić et al. 2006), we can safely utilize another rest-frame color for the selection of the parent sample. In Fig. 8 we show the correlation between $U-B$ and P1 rest-frame colors for all VLA-COSMOS galaxies ($z \leq 1.3$), and derive an analytic relation correlating P1 and $U-B$ (indicated in Fig. 8). The criterion of P1 > 0.15, used to select the VLA-COSMOS AGN sample, corresponds to $U-B > 0.71$. Thus we select the red galaxy parent sample by requiring $I_{auto} \leq 24$, $0.1 < z_{phot} \leq 1.3$, and $U-B > 0.71$. The $U-B$ distribution for all (red and blue) galaxies, that satisfy the magnitude and redshift criteria, is shown in Fig. 9. Note that the adopted $U-B$ threshold, based on the comparison with the $P1$ values, corresponds almost exactly to the $U-B$ value which separates the red from the blue galaxies. Our selection yields 21,525 galaxies in the red galaxy control-parent sample.

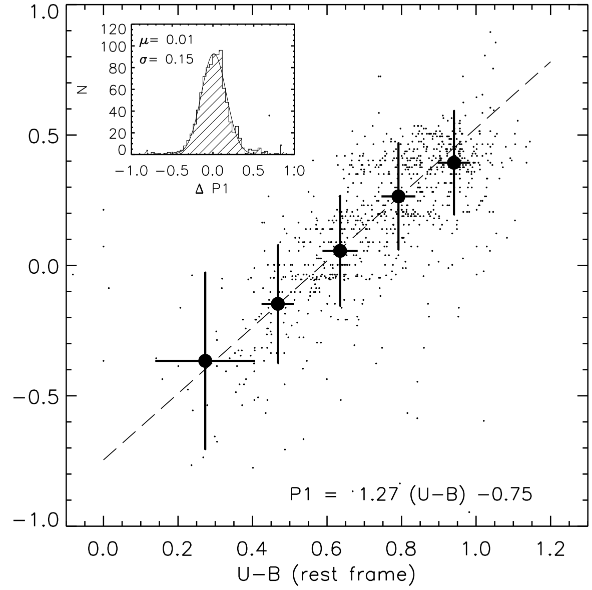

FIG. 8.— Comparison of the P1 and U−B rest frame colors for 941 VLA-COSMOS radio–optical sources (defined in S08a; small dots). The dashed line shows the best linear fit (the analytic form is given in the bottom right of the panel), obtained using the median (P1,U−B) values (large dots). The inset shows the dispersion of the fitted relation, where for a given galaxy Δ P1 is the difference between its P1 value computed using its U−B rest-frame color (obtained by Ilbert et al. 2008) and the one derived directly via SED fitting (as described in S08a).

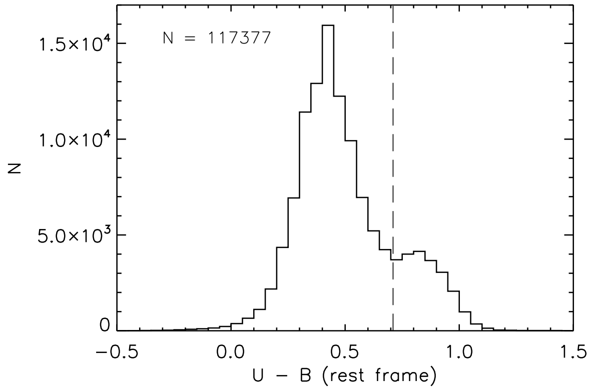

FIG. 9.— $U-B$ rest frame color distribution for 117,377 galaxies ($I_{auto} \leq 24$; $0.1 < z_{phot} \leq 1.3$) drawn from the COSMOS photometric redshift catalog. The red galaxy parent sample of our VLA-COSMOS radio AGN is selected by applying $U-B > 0.71$ (dashed line) to this distribution (this is equivalent to P1 > 0.15 that was used to select our radio AGN; see Fig. 8).

6.2. *The stellar mass properties of VLA-COSMOS AGN*

Using the $1/V_{\rm max}$ method we derive the stellar mass function (SMF) in two redshift bins ($0.2 \leq z \leq 0.7$ and $0.7 < z \leq 1.3$) for both our VLA-COSMOS AGN ($L_{\rm 1.4GHz} \gtrsim 4 \cdot 10^{23}$ W Hz^{-1} which roughly corresponds to a radio volume limited sample), and the red parent galaxy sample. The stellar mass functions are shown in Fig. 10. The SMF for the red galaxy sample agrees well with the recent results based on the GOODS-MUSIC galaxy sample (Fontana et al. 2006). Similarly to what has been shown in the local universe for radio luminous AGN (Best et al. 2005), at intermediate redshifts the SMFs of our radio AGN sample are strongly biased toward high stellar masses. Interestingly, the redshift evolution of the SMFs of the parent galaxy and radio AGN samples is reversed. While for a given stellar mass the comoving number density of red galaxies decreases with redshift, the number density of radio luminous AGN increases. Our results are in good agreement with those of Tasse et al. (2008) based on radio observations of the XMM-LSS field.

We compute the fraction of radio luminous AGN as the ratio of the above derived mass functions in a given stellar mass bin. In Fig. 11 we show the radio AGN fraction as a function of stellar mass in the two adopted red-

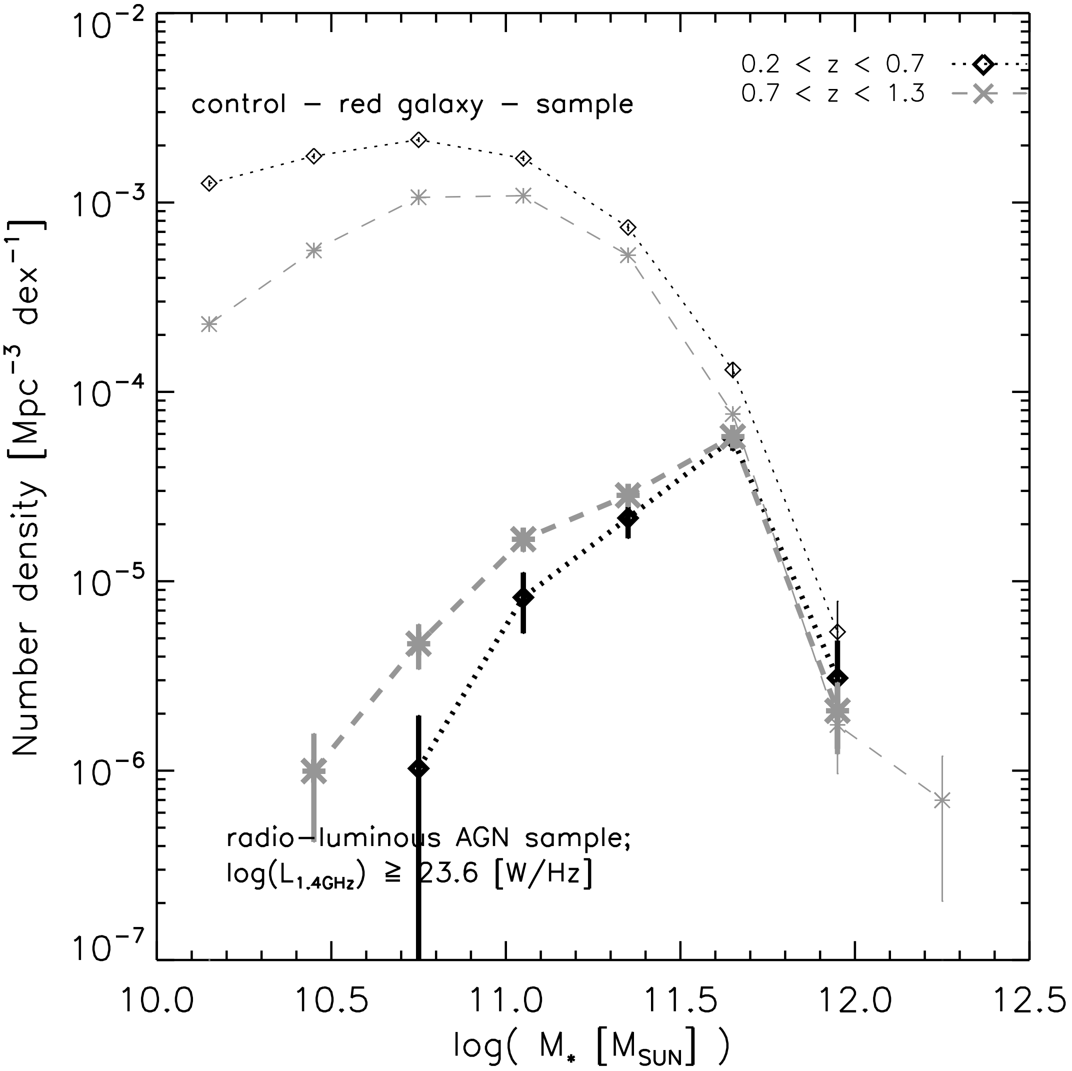

FIG. 10.— Stellar mass function, derived using the $1/V_{\rm max}$ method, of the VLA-COSMOS radio AGN (volume limited, $L_{1.4\rm GHz} \gtrsim 4 \cdot 10^{23}$ W Hz^{-1}; bold symbols) in two redshift ranges, indicated in the panel. For comparison, the stellar mass function of the red, parent galaxy sample in the same redshift ranges is also shown.

shift ranges, and compare it to the results based on the local SDSS and NVSS surveys (Best et al. 2005). The radio AGN fraction in our lower redshift ($0.2 < z < 0.7$) bin agrees remarkably well with the local findings implying insignificant or absent evolution of the radio AGN fraction out to $z \sim 0.7$ at all stellar masses. However, there is a significant change in the fraction of radio luminous AGN at higher redshifts ($0.7 < z < 1.3$), in particular for host galaxies with stellar masses lower than $\log M_* \sim 11.3$. We investigate this further in Sec. 6.4.

6.3. *The star formation quenching rate*

Following Bundy et al. (2008), we define the star formation quenching rate, $\dot{Q}$, as the fraction of all galaxies in a given stellar mass bin that migrate to the red sequence per Gyr. This migration can occur through processes such as mass build up (via 'wet' mergers) or gas consumption (fading of an already massive galaxy to red colors). In Fig. 12 (left panel) we plot the fraction of red galaxies (as defined in Sec. 6.1) relative to the number of all galaxies (see Fig. 9) as a function of cosmic time for various stellar mass bins. The red galaxy fractions have been derived in the same way as the radio AGN fraction (see Sec. 6.2), but using the red and total galaxy samples. The the change in radio fraction per Gyr (α) of this red-galaxy-sequence build-up with cosmic time, shown in the left panel of Fig. 12, is then equivalent to the star formation quenching rate. We find that as stellar mass increases from $\log M_*$ of 10.6 to 11.7 $M_\odot$ $\dot{Q}$ decreases from 6 % Gyr^{-1} to 0.6 % Gyr^{-1}. Note also that for the highest stellar masses the red sequence is already almost fully in place by $z \sim 1$.

6.4. *The triggering rate of low radio-power AGN*

In Sec. 6.3 we have derived the star formation quenching rate based on the build-up of the red galaxy population as a function of cosmic age (left panel in Fig. 12). In the right panel in Fig. 12 we now show the radio vol-

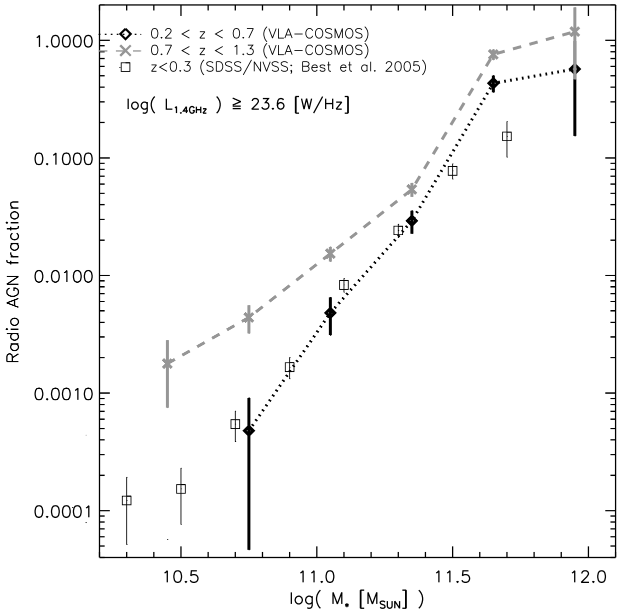

FIG. 11.— Fraction of radio luminous, VLA-COSMOS, AGN ($L_{1.4\mathrm{GHz}} \gtrsim 4 \cdot 10^{23}$ W Hz^{-1}) as a function of stellar mass in two redshift ranges (bold symbols). Also shown is the radio AGN fraction based on the local ($z < 0.3$) SDSS/NVSS samples with the same radio power limit imposed (Best et al. 2005). Note that no evolution of the radio AGN fraction is seen out to $z = 0.7$.

ume limited ($\log L_{1.4\mathrm{GHz}} \geq 23.6$) fraction of our VLA-COSMOS AGN relative to the abundance of the red parent galaxies as a function of cosmic time, for the various stellar mass ranges as shown in Fig. 11. Contrary to the red galaxy fractions, our results yield that the radio AGN fraction decreases with cosmic age. At all stellar masses ($10.6 < \log M_* < 11.7$) a larger fraction of radio luminous AGN is present at earlier, compared to later, cosmic times. Furthermore, the fraction of radio luminous AGN decreases more steeply with cosmic time for higher stellar masses. For example, at $\log M_* \sim 11.65$ the rate of decrease is 10.8 % Gyr^{-1}, while at $\log M_* \sim 10.75$ it is only 0.1 % Gyr^{-1}.

Given the fraction of radio AGN at a given cosmic time, we can estimate the average time that each single massive galaxy spends as a radio AGN, τ_{radio}. Assuming that massive galaxies, that form the parent sample of our radio AGN, form around $z \sim 2.5 - 3$ and survive to $z \sim 0$, their lifetime is then ~ 10 Gyr. Multiplying this lifetime by the fraction of observed radio AGN then yields an approximate estimate of τ_{radio}. At a given cosmic time, τ_{radio}, which is in the range of roughly 10 Myr to 5 Gyr for our VLA-COSMOS AGN (see right panel in Fig. 12), is thus related either to the average duration of a single radio-episode or to the frequency of radio mode re-triggering.

Independent calculations of radio source lifetimes, t_{radio}, result in lifetimes of a few times 0.001 Gyr to a few times 0.1 Gyr (Alexander & Leahy 1987; Shabala et al. 2008). Assuming that the radio source lifetime does not significantly change with cosmic time, it is most likely that the computed τ_{radio} reflects the occurrence of multiple radio-phases of a single massive galaxy at a certain cosmic time. A radio 'on' phase of 0.001-0.1 Gyr, combined with the derived τ_{radio}, implies then that radio AGN activity has been triggered more often in the past than it is today, and that at a given cosmic time it is more often triggered in massive galaxies compared to lower mass galaxies.

The *minimum* radio AGN triggering rate can be obtained by assuming the maximum t_{radio} of 0.1 Gyr, and taking into account the above derived τ_{radio} (0.010 − 5 Gyr). It is then 0.1 % Gyr^{-1} to 50 % Gyr^{-1} for the lowest and highest stellar mass bins, respectively. Yet, in the previous section we have computed a star formation quenching rate of 6 % Gyr^{-1} for the lowest and 0.6 % Gyr^{-1} for the highest stellar mass bins (see left panel in Fig. 12). Hence, comparing these estimates yields that our derived radio AGN triggering rates are by many factors off the derived star formation quenching rates, especially for the highest stellar masses.

If the quenching of star formation, that causes the build-up of the red galaxy sequence, is related to a *single* episode (i.e. once the star formation is suppressed it does not restart at a significant level), then it is highly unlikely that a direct connection between the two phenomena – the *low radio power* AGN triggering and the star formation quenching rates – exists. However, these results do not exclude the possibility that low radio power AGN are responsible for preventing the galaxies to grow higher in mass, once they have been established as the most massive 'red-and-dead' galaxies, as has been proposed in numerous cosmological models (Croton et al. 2006; Bower et al. 2006; Sijacki & Springel 2006; Sijacki et al. 2007). This will be further explored in Sec. 7.3.

7. IMPLICATIONS FOR GALAXY FORMATION

7.1. *High and low radio power AGN: Different stages of galaxy evolution*

In the last decades studies at various wavelength regimes have converged towards a widely accepted galaxy formation picture. Galaxies are thought to evolve in time from an initial stage with spiral morphology and blue optical colors towards elliptical morphologies with red optical colors (Bell et al. 2004a,b; Borch et al. 2006; Faber et al. 2007; Brown et al. 2007; Hopkins et al. 2007). This evolution is not linear but happens through interspersed episodes of massive mass accretion onto the stellar body as well as their central massive black holes seen as quasars (Sanders & Mirabel 1996; Sanders 2003). The blue-to-red galaxy evolution is accompanied with significant build-up of stellar and BH mass; the reddest galaxies observed in the universe are also the oldest and the most massive ones ($M_* \gtrsim 10^{11}$ $\mathrm{M}_\odot$; e.g. Baldry et al. 2004, 2006; Faber et al. 2007). Mergers between galaxies, rich in cold gas ('wet' mergers), appear to be one of the key processes governing this mass build-up and the blue-to-red galaxy transformation (Sanders 2003; Bell et al. 2004a,b; Borch et al. 2006; Faber et al. 2007; Brown et al. 2007). Furthermore, mergers are considered to be the major drivers of the growth of super-massive black holes in the centers of galaxies (Kauffmann & Haehnelt 2000; Croton et al. 2006) as they enable large amounts of gas to be funneled to, and accrete onto the central BH.

In the context of the general picture of galaxy evolution, the following scenario for the evolution of radio AGN seems very plausible. High radio power AGN are

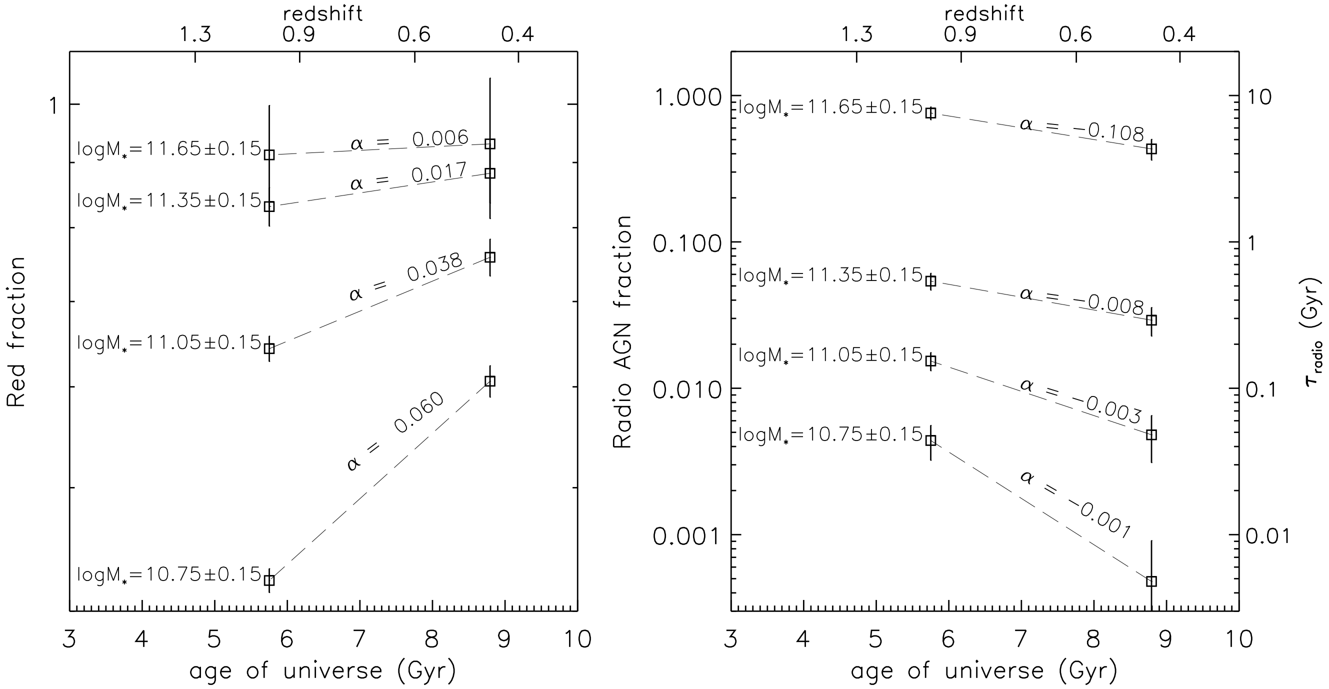

FIG. 12.— Left panel: The fraction of red galaxies ($P1 > 0.15$; equivalent to $U - B > 0.71$; left panel), compared to all galaxies, as a function of cosmic age for different stellar mass ranges (indicated in the panel). The right panel shows the fraction of radio AGN in the red, parent galaxy sample (as defined in the text) as a function of cosmic age for the various stellar mass bins. The fractional change with cosmic time has been characterized with a linear slope (α), which is indicated for each stellar mass bin. The radio AGN fraction can be related to the average time a galaxy spends as a radio AGN ($\tau_{\rm radio}$; see text for details), shown on the right-hand y-axis in the right panel. Note the different y scales in the left and right panels. Note also that there is no correspondence between the increase of the red galaxy fraction, and the decrease of the radio AGN fraction with cosmic time.

preferably found in galaxies that have not yet reached the highest stellar masses and show a strong decline with time of their number density. On the other hand, the hosts of low power radio AGN are generally old massive 'red-and-dead' galaxies and have an almost constant space density. This implies that the radio triggering mechanism in a galaxy is a strong function of the host galaxy's properties and it is likely that it is linked to different stages during the formation of massive old galaxies. In this scenario the occurrence of the two radio modes would be naturally linked to the overall galaxy formation process and their impact and timescales could be observationally constrained.

In particular, the HERAGN phase seems to be closely tied to major merger remnants (as many hosts are found to be disturbed, have blue colors and show signs of on-going star formation; e.g. Heckman et al. 1986; Baum et al. 1992), as well as significant black hole growth (supported by high − ∼ Eddington − accretion rates observed; see Sec. 5). These major mergers are critical for the formation of massive ellipticals. On the other hand, the LERAGN phase is mainly observed in the most massive galaxies, where a mechanism is required (Croton et al. 2006; Bower et al. 2006) which prevents intra-cluster gas from cooling onto the massive host galaxy. The properties of LERAGN such as lower amounts of gas and dust compared to HERAGN (de Koff et al. 1996; Leon et al. 2001; Müller et al. 2004; Evans et al. 2006; Emonts et al. 2008), a modest BH growth (Evans et al. 2006; Hopkins et al. 2006a; Cao 2007; Hardcastle et al. 2007), and fully built up stellar and BH masses already at $z \sim 1$ (Sec. 5, Kauffmann et al. 2008), support this interpretation.

In the context of the generally adopted red galaxy formation scenario, our results thus suggest that high-excitation radio AGN (i.e. high radio-power AGN; $L_{1.4\rm GHz} \gtrsim 10^{25}$ W Hz^{-1}) occur in a stage of galaxy evolution presumably after a gas-rich merger which induces a phase of significant black hole growth. This active radio phase may last $10^6 - 10^7$ yr (e.g. Alexander & Leahy 1987, Shabala et al. 2008). Within the post-merging process the accumulated cold gas will be consumed by the host galaxy via star-formation and/or black-hole accretion. Low-excitation radio AGN (i.e. low radio power AGN; $L_{1.4\rm GHz} \lesssim 10^{25}$ W Hz^{-1}) then represent a later stage of the galaxy formation process, when the amount of cold gas in the host has already been reduced. In this phase the galaxy's BH is accreting quiescently in a radiatively inefficient way, i.e. below a certain critical accretion rate in Eddington units, and most of the released energy is in kinetic form (see e.g. Hardcastle et al. 2007; Merloni & Heinz 2008). This radio phase lasts a few times 10^7 yr to a few times 10^8 yr (e.g. McNamara et al. 2005; Nulsen et al. 2005). Thus, our results imply that high radio power AGN appear in an early stage, while low radio power occur in a late stage in the evolution of massive galaxies.

The evolution of the integrated luminosity density, shown in Fig. 4, can be well explained in our scenario. This diagram can be interpreted as the evolution of $\Omega_{1.4\rm GHz}$ for two radio luminous, but fundamentally different, types of galaxies where the HERAGN and LER-

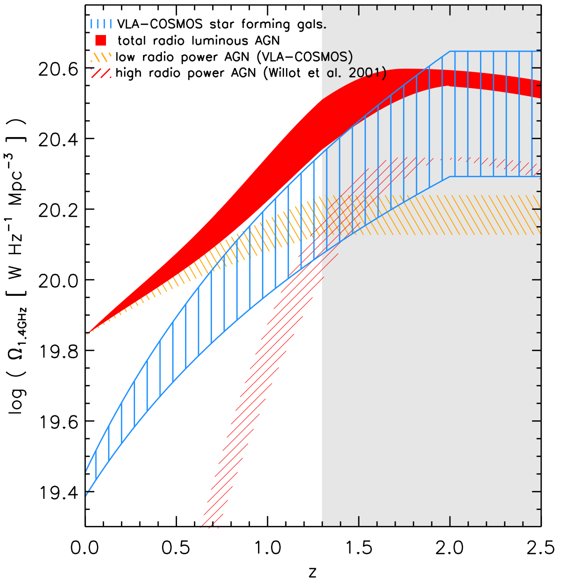

Fig. 13.— Evolution of the comoving 20 cm integrated luminosity density ($\Omega_{1.4\mathrm{GHz}}$) for *all* radio AGN (filled red curve) and star forming galaxies (vertically blue hatched curve) since $z = 2.5$. The evolution of $\Omega_{1.4\mathrm{GHz}}$ for the total AGN population is a superposition of the evolution of low (VLA-COSMOS; orange hatched curve) and high (model taken from Willott et al. 2001; red hatched region) radio power AGN. The light-gray shaded area of the plot shows the redshift range where the evolution of the VLA-COSMOS AGN and star forming galaxies has been extrapolated ($z > 1.3$; see text for details).

AGN reflect modes of vigorous and modest BH growth, respectively.

The luminosity density of the HERAGN equivalent to a mode of vigorous BH growth evolves dramatically since $z = 1.3$, consistent with e.g. the evolution of optically and X-ray selected quasars (see Willott et al. 2001; see also Boyle et al. 2000 and Ueda et al. 2003). The state of modest black hole growth (in our case the LERAGN) evolves significantly slower, and it dominates the total comoving AGN radio power output at low redshifts ($z \lesssim 0.7$). At these redshifts the most massive, 'red-and-dead', often central cluster galaxies associated with radio sources, are already in place (e.g. Blakeslee et al. 2003) thus providing an optimal environment for a self-regulating process of modest BH growth (at sub-Eddington accretion rates) and low radio power AGN activity.

In summary, *the evolution of a radio selected AGN population seems to be consistent with the possibly bimodal evolution of black hole accretion modes (modest vs. vigorous) that occur during different stages in the process of the formation of (massive) galaxies.*

7.2. *The co-evolution of star formation and radio AGN activity in radio luminous galaxies*

Black hole growth, especially merger driven growth, is expected to be linked to starburst activity (Sanders & Mirabel 1996; Boyle & Terlevich 1998; Franceschini et al. 1999; Sanders 2003; Croton et al. 2006). Thus, in Fig. 13 we compare the evolution of the integrated comoving 1.4 GHz luminosity density for the VLA-COSMOS star forming galaxies (see S08b for details) and the total radio AGN population, likely reflecting two separate modes of black hole accretion, as argued above. For the latter, $\Omega_{1.4\mathrm{GHz}}$ has been obtained by co-adding the contributions of the low-power (VLA-COSMOS) and the high radio-power AGN (Willott et al. 2001; see Fig. 4).

As the peak of the cosmic star formation and AGN activity occurs at $z > 1$ (Hopkins 2004), we extrapolate $\Omega_{1.4\mathrm{GHz}}$ to $z = 2.5$ as follows. For the high-power AGN we use the Willott et al. (2001) model which is well constrained by 3CRR, 6CE, and 7CRS data at $z < 3$ (see Fig. 1 in Willott et al. 2001). As can be seen from Fig. 3, the full (weak plus powerful radio AGN) Willott et al. model describes well also the evolution of weak radio AGN, at least at $z < 1.3$. Here we assume that this is the case also for $z > 1.3$. Thus, in order to be consistent with this model, in which the low-power AGN population is assumed to stop evolving beyond a certain redshift, we assume that the comoving volume densities of VLA-COSMOS AGN remains constant for $z>1.3$. Note however that this may not necessarily be realistic if the comoving volume density of low-luminosity AGN exhibits a turn-over, but at lower redshift compared to powerful radio sources (e.g. Waddington et al. 2001).

To extrapolate $\Omega_{1.4\mathrm{GHz}}$ for the star forming galaxies we follow Hopkins (2004) who showed, based on a compilation of numerous studies based on independent data sets, that ceasing the evolution beyond $z = 2$ (given the evolving radio luminosity function for star forming galaxies) reproduces the observed cosmic star formation history well (see e.g. Fig. 1 in Hopkins 2004). Thus, our extrapolation of $\Omega_{1.4\mathrm{GHz}}$ beyond $z = 1.3$ is fairly robust as it is based on independent results drawn from various data sets that constrain these cosmic times well.

The integrated comoving 20 cm luminosity density for radio luminous star forming and AGN galaxies, shown in Fig. 13, appears to evolve coevally at high redshifts ($0.7 \lesssim z < 2.5$), where powerful AGN significantly contribute to the $\Omega_{1.4\mathrm{GHz}}$. Both seem to flatten in the redshift range of about $1.5 - 2$. Although not conclusive, this is suggestive of a link between the process of star formation and radio AGN activity (see also e.g. Boyle & Terlevich 1998; Franceschini et al. 1999. This can be understood in the scenario of galaxy formation where gas-rich mergers of spiral galaxies govern the formation of gas-poor elliptical galaxies. As the galaxies merge, the bulk of their cold gas, that was originally distributed throughout the disk of the merging constituents, is funneled into the inner few kpc of the merging system and fuels both star formation and AGN activity (possibly sequentially; Sanders 2003). Thus, co-evolution of star forming and powerful radio AGN activity is predominantly expected in systems with significant amounts of cold gas, consistent with the properties found in high-excitation radio AGN.

On the other hand, the evolution of the integrated comoving 20 cm luminosity density for star forming and radio AGN galaxies decouples below $z \sim 0.7$ (see Fig. 13) where low radio power AGN with modest BH growth dominate the total AGN radio-power output in the universe (see Fig. 4). In the context of our high-to-low-radio-power transition scenario proposed in the previous section, this AGN activity is triggered in a later evolutionary stage of a massive galaxy (corresponding to LERAGN), where a large fraction of the gas reservoir has already been consumed. Thus, a close link between star formation and AGN activity is not expected in this regime. Such an expectation is also supported by our results on the quenching of star formation in the context of the build-up of the red galaxy sequence, derived in Sec. 6.3. We have shown that processes causing the star formation quenching are not likely to be also governing the triggering of low radio power AGN phases. If they are responsible for the decline in the star formation rate density since $z \sim 1$ (at least at the high stellar mass end; see e.g. S08b), then no connection between $\Omega_{\rm 1.4GHz}$ for low-power radio AGN and star forming galaxies is expected.

We would like to stress that the radio energy injection into the surrounding medium of such quiescent modes of black hole accretion has been invoked in numerous cosmological models (e.g. Croton et al. 2006; Bower et al. 2006; Sijacki & Springel 2006; Sijacki et al. 2007) as the main heating mechanism responsible for preventing further star formation in the given host galaxy (assuming that every massive red galaxy undergoes a phase of radio AGN activity). This process was the key ingredient that allowed a good reproduction of e.g. the high mass end of the galaxy stellar mass function in the models. To shed light on the plausibility of such a process we explore in the next section the injection energies of our VLA-COSMOS AGN, and compare them to the recipes used in cosmological simulations.

7.3. *The evolution of radio AGN feedback in massive galaxies*

In this section we derive the mechanical energy injected into the surrounding medium by low-power (VLA-COSMOS) radio AGN, which are possible candidates for preventing star formation in massive galaxies as proposed in recent cosmological models (Croton et al. 2006; Bower et al. 2006; Sijacki & Springel 2006; Sijacki et al. 2007), and defined as 'radio mode' (see Croton et al. 2006 for details).

Monochromatic radio luminosity is not a direct indicator of the mechanical energy output of a radio galaxy into its surrounding medium. The latter can be estimated making use of the observed interplay in galaxy clusters between radio galaxies and the hot X-ray emitting intra-cluster gas, where radio jets induce cavities in the hot gas and inflate buoyantly rising bubbles (see e.g. Bîrzan et al. 2004; Allen et al. 2006; Bîrzan et al. 2008). As the total energy within a bubble is the sum of its internal energy and the PdV work done by its inflation, the mechanical radio luminosity is given by the ratio of this total energy and the age of the bubble (see e.g. Bîrzan et al. 2004; Allen et al. 2006; Bîrzan et al. 2008). Using mechanical luminosities derived by Bîrzan et al. (2004) for a sample of 18 radio galaxies in clusters or groups, Best et al. (2006) have found that the relation of mechanical and monochromatic radio power is best described by a power-law, however with a large scatter (see Fig. 1 and eq. 2 in Best et al. 2004). Based on this relation, they have computed the total comoving volume averaged mechanical heating rate, $\Omega_{\rm L\,mech}$, in the local universe provided by radio luminous AGN, which was found to be a factor of 10-20 lower than the local density of radio mode heating predicted in the Croton et al. (2006) semi-analytic model.

Here we follow the prescription of Best et al. (2006) to estimate the evolution of $\Omega_{\rm L\,mech}$, using the most recent calibration for the conversion of monochromatic radio to mechanical power (Bîrzan et al. 2008). First, at each redshift we convert the radio AGN monochromatic luminosity function (given by our best fit PLE and PDE models; see Sec. 4.1) into a mechanical luminosity density function using eq. 16, given by Bîrzan et al. (2008). Then we integrate it above a minimum mechanical luminosity equivalent to $\rm L_{1.4GHz} = 10^{21}$ W Hz^{-1}. The resulting evolution of $\Omega_{\rm L\,mech}$ is shown in Fig. 14, where we compare it to the density of the radio mode heating given in the Croton et al. (2006) cosmological model. The latter has been obtained from Fig. 3 in Croton et al., where we converted their comoving black hole accretion rate density, $\dot{m}_{\rm BH}$ (shown on the right-hand side of the y axis), into the volume-averaged heating rate utilizing $\Omega_{\rm L\,mech} = \eta\, \dot{m}_{\rm BH}\, c^2$; where η is the standard efficiency of the conversion of mass into energy ($\eta = 0.1$), and c is the speed of light (see also eq. 11 of Croton et al. 2006).

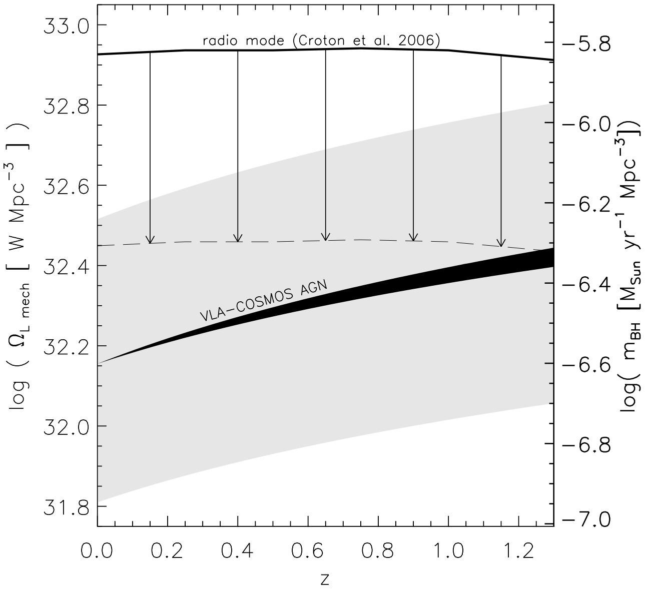

Fig. 14.— The cosmic evolution of the volume averaged mechanical heating rate $\Omega_{\rm L\,mech}$ for low-power VLA-COSMOS AGN, which are likely candidates for the 'radio mode' heating invoked in cosmological models (filled curve). The volume averaged accretion rate is shown on the right-hand side y-axis (see text for details). The uncertainties in the correlation between $\rm L_{1.4GHz}$ and $\rm L_{mech}$ (given in Bîrzan et al. 2008) are illustrated by the light-gray shaded area. Also shown is the evolution predicted in the Croton et al. (2006) semi-analytic model (thick line), and its possible value lowered by a factor of 2-3 (indicated by arrows) due to a systematic over-estimation of the heating rate in the model (see text for details).

It is important to note that both the model- and observation-based heating rates are subject to large uncertainties. The model cooling rates are likely to be overestimated by a factor of 2-3 (indicated in Fig. 14) due to the nature of the underlying cooling flow model (Best et al. 2006). On the other hand, the observationally derived heating rates have uncertainties of the order of ~ 0.8 dex due to the scatter in the conversion of monochromatic to mechanical radio luminosities. Furthermore, they may be strongly under-estimated (up to a factor of 6) as the work done during the inflation of a bubble may be significantly higher than the reversible pdV work usually assumed in the computation of mechanical luminosities (see Binney et al. 2007 for details). In addition, the minimum mechanical power equivalent to $L_{1.4\mathrm{GHz}} = 10^{21}$ W Hz^{-1} has been chosen rather arbitrarily. For example, a lower threshold would yield a higher $\Omega_{\mathrm{L\,mech}}$. Nonetheless, the qualitative agreement between the model and observations seen in Fig. 14 is encouraging for the idea that radio luminous AGN play an important role in the process of galaxy evolution.

Based on two samples of local massive red galaxies with available optical, radio and X-ray observations, Best et al. (2006) have shown that radio source activity may indeed control the growth rate of the host galaxy, as has been proposed in cosmological models. Best et al. have found that, across a wide range of stellar masses, the radio source heating rate agrees remarkably well with the cooling rate of the host galaxy's surrounding hot gas halo. Averaged over time, the recurring radio source activity can then balance the radiative losses from its surrounding hot gas halo and thereby suppress the cooling of the gas, and in this way control the growth rate of the galaxy (see e.g. Croton et al. 2006). Here we have shown that various properties of $z \sim 1$ (low power) radio AGN are comparable to the properties of local radio AGN. Thus it is very likely that the same radio heating – hot gas cooling interplay, observed locally, takes place also in $z \sim 1$ radio AGN. This then strongly argues in favor of the plausibility that (low-power) radio AGN activity (i.e. 'radio mode') is a key factor that prevents further mass growth in massive 'red-and-dead' galaxies across cosmic times, at least since ~ 4.5 Gyr after the Big Bang.

8. SUMMARY AND CONCLUSIONS

Using the largest sample of low luminosity radio AGN at intermediate redshifts available to-date drawn from the VLA-COSMOS survey, we explored the evolution and composition of the radio AGN population out to a redshift of z∼1. In particular, we derived the radio AGN luminosity function in several redshift bins. Compared to powerful ($L_{1.4\mathrm{GHz}} > 5 \times 10^{25}$ W Hz^{-1}) radio AGN the low radio power ($L_{1.4\mathrm{GHz}} \lesssim 5 \times 10^{25}$ W Hz^{-1}) AGN probed here show only a weak decline in their luminosity density since $z = 1.3$.

An analysis of the host properties of weak and powerful radio AGN shows that they form two relatively distinct classes, with powerful radio AGN being related to modes of vigorous BH growth whereas weak radio AGN are related to only modest BH growth. This is also reflected in the types of host galaxies with weak radio AGN being preferentially found in the most massive and evolved galaxies (even out to z∼1).

Joint analysis of the evolution of the 20 cm luminosity density of the AGN and the star formation rate density suggests that the powerful radio sources are preferably triggered in major mergers following shortly after the phase of massive star formation at high redshifts. This would also naturally explain the strong decline of these sources below a redshift of z=1. As the volume density of weak radio AGN stays fairly constant, they can significantly contribute to the heating of the their surrounding medium and thus inhibit gas accretion onto their host galaxies as recently suggested for the radio mode in cosmological models.

The authors are grateful to P. N. Best for especially deriving the SDSS/NVSS radio source fractions as a function of stellar mass with a radio luminosity cut that matches the VLA-COSMOS survey data. CC acknowledges support from the Max-Planck Society and the Alexander von Humboldt Foundation through the Max-Planck-Forschungspreis 2005. GZ and SB acknowledge support from an INAF contract PRIN-2006/1.06.10.08 and an ASI grant ASI/COFIS I/026/07/0. TP acknowledges support from PSC-CUNY grant # 69612-00 38.

REFERENCES

Allen, S. W., Dunn, R. J. H., Fabian, A. C., Taylor, G. B., & Reynolds, C. S. 2006, MNRAS, 372, 21

Auger, M. W., Becker, R. H., & Fassnacht, C. D. 2008, AJ, 135, 1311

Baldi, R. D., & Capetti, A. 2008, A&A, 489, 989

Baldry, I. K., Glazebrook, K., Brinkmann, J., Ivezić, Ž., Lupton, R. H., Nichol, R. C., & Szalay, A. S. 2004, ApJ, 600, 681

Baldry, I. K., Balogh, M. L., Bower, R. G., Glazebrook, K., Nichol, R. C., Bamford, S. P., & Budavari, T. 2006, MNRAS, 373, 469

Baldwin, J. A., Phillips, M. M., & Terlevich, R. 1981, PASP, 93, 5

Barger, A. J., Cowie, L. L., & Wang, W.-H. 2007, ApJ, 654, 764

Barthel, P. D. 1989, ApJ, 336, 606

Baum, S. A., Heckman, T. M., & van Breugel, W. 1992, ApJ, 389, 208

Bell, E. F., et al. 2004a, ApJ, 608, 752

Bell, E. F., et al. 2004b, ApJ, 600, L11

Best, P. N., et al. 2005, MNRAS, 362, 9

Best, P. N., Kaiser, C. R., Heckman, T. M., & Kauffmann, G. 2006, MNRAS, 368, L67

Bîrzan, L., Rafferty, D. A., McNamara, B. R., Wise, M. W., & Nulsen, P. E. J. 2004, ApJ, 607, 800

Bîrzan, L., McNamara, B. R., Nulsen, P. E. J., Carilli, C. L., & Wise, M. W. 2008, ArXiv e-prints, 806, arXiv:0806.1929

Blakeslee, J. P., et al. 2003, ApJ, 596, L143

Bondi, E., et. al. 2008, accepted for publication in AJ; arXiv:0804.1706

Bower, R. G., Benson, A. J., Malbon, R., Helly, J. C., Frenk, C. S., Baugh, C. M., Cole, S., & Lacey, C. G. 2006, MNRAS, 370, 645

Boyle, B. J., & Terlevich, R. J. 1998, MNRAS, 293, L49

Borch, A., et al. 2006, A&A, 453, 869

Brown, M. J. I., Dey, A., Jannuzi, B. T., Brand, K., Benson, A. J., Brodwin, M., Croton, D. J., & Eisenhardt, P. R. 2007, ApJ, 654, 858

Brusa, M., et al. 2008, submitted

Bruzual, G., & Charlot, S. 2003, MNRAS, 344, 1000

Cao, X. 2007, ApJ, 659, 950

Capak, E., et. al. 2007, ApJS, COSMOS special issue, in press

Chabrier, G. 2003, PASP, 115, 763

Chiaberge, M., Capetti, A., & Macchetto, F. D. 2005, ApJ, 625, 716

Clewley, L., & Jarvis, M. J. 2004, MNRAS, 352, 909

Condon, J. J. 1989, ApJ, 338, 13

Condon, J. J., Cotton, W. D., & Broderick, J. J. 2002, AJ, 124, 675

Croton, D. J., et al. 2006, MNRAS, 365, 11

Cowie, L. L., Barger, A. J., Fomalont, E. B., & Capak, P. 2004, ApJ, 603, L69

Daddi, E., et al. 2007, ArXiv e-prints, 705, arXiv:0705.2832

de Koff, S., Baum, S. A., Sparks, W. B., Biretta, J., Golombek, D., Macchetto, F., McCarthy, P., & Miley, G. K. 1996, ApJS, 107, 621

Donoso, E., Best, P. N., & Kauffmann, G. 2008, arXiv:0809.2076

Dunlop, J. S., & Peacock, J. A. 1990, MNRAS, 247, 19

Emonts, B., Morganti, R., Oosterloo, T., & van Gorkom, J. 2008, ArXiv e-prints, 801, arXiv:0801.4769

Evans, D. A., Worrall, D. M., Hardcastle, M. J., Kraft, R. P., & Birkinshaw, M. 2006, ApJ, 642, 96

Faber, S. M., et al. 2007, ApJ, 665, 265

Fabian, A. C. 1994, ARA&A, 32, 277

Fanaroff, B. L. and Riley, J. M., 1074, MNRAS, 167, 31

Finoguenov, A., et al. 2007, ApJS, 172, 182

Fontana, A., et al. 2006, A&A, 459, 745

Franceschini, A., Hasinger, G., Miyaji, T., & Malquori, D. 1999, MNRAS, 310, L5

Haas, M., et al. 2004, A&A, 424, 531

Hardcastle, M. J., Evans, D. A., & Croston, J. H. 2006, MNRAS, 370, 1893

Hardcastle, M. J., Evans, D. A., & Croston, J. H. 2007, MNRAS, 376, 1849

Heckman, T. M., Smith, E. P., Baum, S. A., van Breugel, W. J. M., Miley, G. K., Illingworth, G. D., Bothun, G. D., & Balick, B. 1986, ApJ, 311, 526

Hine, R. G., & Longair, M. S. 1979, MNRAS, 188, 111

Hopkins, A. M. 2004, ApJ, 615, 209

Hopkins, P. F., Narayan, R., & Hernquist, L. 2006, ApJ, 643, 641

Hopkins, P. F., Robertson, B., Krause, E., Hernquist, L., & Cox, T. J. 2006, ApJ, 652, 107

Hopkins, P. F., Bundy, K., Hernquist, L., & Ellis, R. S. 2007, ApJ, 659, 976

Huynh, M. T., et al. (2008); accepted for publication in AJ; arXiv:0803.4394

Ilbert, O., et al. 2008, submitted

Kauffmann, G., & Haehnelt, M. 2000, MNRAS, 311, 576

Kauffmann, G., Heckman, T. M., & Best, P. N. 2008, MNRAS, 384, 953

Körding, E. G., Jester, S., & Fender, R. 2008, MNRAS, 383, 277

Lacy, M., et al. 2004, ApJS, 154, 166

Laing, R. A., Jenkins, C. R., Wall, J. V., & Unger, S. W. 1994, The Physics of Active Galaxies, 54, 201

Ledlow, M. J., & Owen, F. N. 1996, AJ, 112, 9

Le Floc'h, E., et al. 2005, ApJ, 632, 169

Leon, S., Lim, J., Combes, F., & van-Trung, D. 2001, QSO Hosts and Their Environments, 185

Lim, J., Leon, S., Combes, F., & Dinh-v-Trung 2003, Active Galactic Nuclei: From Central Engine to Host Galaxy, 290, 529

Marconi, A., & Hunt, L. K. 2003, ApJ, 589, L21

Mauch, T., & Sadler, E. M. 2007, MNRAS, 375, 931

McLure, R. J., & Dunlop, J. S. 2002, MNRAS, 331, 795

McLure, R. J., & Dunlop, J. S. 2004, MNRAS, 352, 1390

McNamara, B. R., Nulsen, P. E. J., Wise, M. W., Rafferty, D. A., Carilli, C., Sarazin, C. L., & Blanton, E. L. 2005, Nature, 433, 45

Merloni, A., & Heinz, S. 2008, MNRAS, 388, 1011

Müller, S. A. H., Haas, M., Siebenmorgen, R., Klaas, U., Meisenheimer, K., Chini, R., & Albrecht, M. 2004, A&A, 426, L29

Nulsen, P. E. J., McNamara, B. R., Wise, M. W., & David, L. P. 2005, ApJ, 628, 629

Obrić, M., et al. 2006, MNRAS, 370, 1677

Owen, F. N. 1993, Jets in Extragalactic Radio Sources, 421, 273

Sadler, E. M., et al. 2002, MNRAS, 329, 227

Sadler, E. M., et al. 2007, MNRAS, 381, 211

Sanders, D. B., & Mirabel, I. F. 1996, ARA&A, 34, 749

Sanders, D. B. 2003, Journal of Korean Astronomical Society, 36, 149

Schinnerer, E., et. al. 2007, ApJS, COSMOS special issue, in press

Schmidt, M. 1968, ApJ, 151, 393

Schmidt, M., Schneider, D. P., & Gunn, J. E. 1995, AJ, 110, 68

Scoville, E., et. al. 2007, ApJS, COSMOS special issue, in press

Sijacki, D., & Springel, V. 2006, MNRAS, 366, 397

Sijacki, D., Springel, V., di Matteo, T., & Hernquist, L. 2007, MNRAS, 380, 877

Silverman, J. D., et al. 2008, ApJ, 679, 118

Smolčić, V., et al. 2006, MNRAS, 371, 121

Smolčić, V., et al. 2007, ApJS, 172, 295

Smolčić, V., et al. 2008, accepted for publication in ApJS, arXiv:0803.0997; S08a

Smolčić, V., et al. 2008, accepted for publication in ApJ; S08b

Solomon, P. M., & Vanden Bout, P. A. 2005, ARA&A, 43, 677

Stern, D., et al. 2005, ApJ, 631, 163

Tasse, C., Best, P. N., Röttgering, H., & Le Borgne, D. 2008, A&A, 490, 893

Trump, J. R., et al. 2007, ApJS, 172, 383

Waddington, I., Dunlop, J. S., Peacock, J. A., & Windhorst, R. A. 2001, MNRAS, 328, 882

White, S. D. M., & Rees, M. J. 1978, MNRAS, 183, 341

White, S. D. M., & Frenk, C. S. 1991, ApJ, 379, 52

Willott, C. J., Rawlings, S., Blundell, K. M., Lacy, M., & Eales, S. A. 2001, MNRAS, 322, 536